



저작자표시 2.0 대한민국

이용자는 아래의 조건을 따르는 경우에 한하여 자유롭게

- 이 저작물을 복제, 배포, 전송, 전시, 공연 및 방송할 수 있습니다.
- 이차적 저작물을 작성할 수 있습니다.
- 이 저작물을 영리 목적으로 이용할 수 있습니다.

다음과 같은 조건을 따라야 합니다:



저작자표시. 귀하는 원저작자를 표시하여야 합니다.

- 귀하는, 이 저작물의 재이용이나 배포의 경우, 이 저작물에 적용된 이용허락조건을 명확하게 나타내어야 합니다.
- 저작권자로부터 별도의 허가를 받으면 이러한 조건들은 적용되지 않습니다.

저작권법에 따른 이용자의 권리는 위의 내용에 의하여 영향을 받지 않습니다.

이것은 [이용허락규약\(Legal Code\)](#)을 이해하기 쉽게 요약한 것입니다.

[Disclaimer](#) 

Prodrug BMP-7 attenuates pulmonary fibrosis through
downregulation of bone marrow derived Apo E⁺ alveolar
macrophage

Nam Eun Kim

The Graduate School
Yonsei University
Department of Medicine

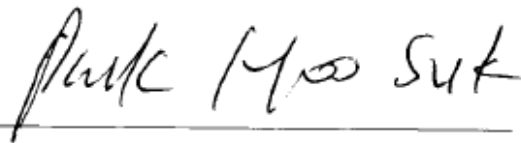
Prodrug BMP-7 attenuates pulmonary fibrosis through
downregulation of bone marrow derived Apo E⁺ alveolar
macrophage

A Dissertation Submitted
to the Department of Medicine
and the Graduate School of Yonsei University
in partial fulfillment of the
requirements for the degree of
Doctor of Philosophy in Medical Science

Nam Eun Kim

June 2024

**This certifies that the Dissertation
of Nam Eun Kim is approved.**



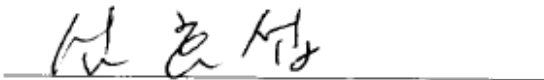
Thesis Supervisor Moo Suk Park



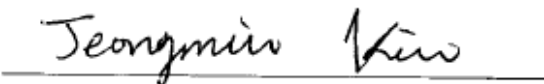
Thesis Committee Member Jong In Yook



Thesis Committee Member Jong Wook Shin



Thesis Committee Member Hyo Sup Shim



Thesis Committee Member Jeongmin Kim

**The Graduate School
Yonsei University
June 2024**

ACKNOWLEDGEMENTS

본 논문이 완성되기까지 방향을 제시해주시고 지도 해주신 박무석 교수님께 존경과 감사의 인사를 올립니다. 바쁘신 중에도 면밀하게 논문 심사를 맡아 주시고 조언해주신 육종인 교수님 감사합니다. 더불어 김현실 교수님, 조수민 박사님께 감사드리고, 실험을 도와주신 많은 분들께 감사하다는 말씀을 전하고 싶습니다.

마지막으로 저를 항상 지지해주시는 든든한 부모님과 열심히 공부중인 동생에게 박사학위 취득의 영광을 돌리도록 하겠습니다. 감사합니다.

TABLE OF CONTENTS

ABSTRACT IN ENGLISH	
1. INTRODUCTION.....	1
2. MATERIALS AND METHODS.....	2
2.1. Preparation of prodrug of BMP-7	2
2.2. <i>In vivo</i> distribution analysis	3
2.3. Experiments groups	3
2.4. Method of experiments	3
2.4.1 Isolation of bronchoalveolar lavage cells and cell counts	3
2.4.2. Lung tissue harvest and histological examination	4
2.4.3. Western blotting	4
2.4.4. ELISA	4
2.4.5. Single cell RNA-seq analysis of BAL fluid cells	5
2.4.6. Immunofluorescence & Immunohistochemistry staining	5
2.5. Statistics.....	6
2.6. Study approval.....	6
3. RESULTS	7
3.1. Prodrug BMP-7 is delivered to the peripheral lung and shows tissue retention..	7
3.2. Prodrug BMP-7 attenuates BLM-induced pulmonary fibrosis.....	9
3.3. Prodrug BMP -7 inhibits the TGF- β /Smad2/3 signaling pathway.....	11
3.4. Prodrug BMP-7 attenuates pulmonary fibrosis by suppressing chemokines.....	13
3.5. Prodrug BMP-7 changes the composition of inflammatory cells in the BALF of BLM- induced lung fibrosis mouse model	15
3.6. Prodrug BMP-7 changes ApoE expression with macrophages in a BLM-induced fibrosis mouse model and normal and IPF human lung tissues	19
4. DISCUSSION	22
5. CONCLUSION	24
REFERENCES.....	25
APPENDICES.....	30

ABSTRACT(INKOREAN)41

LIST OF FIGURES

<Fig 1> <i>In vivo</i> IVIS imaging	8
<Fig 2> Inhaled prodrug BMP-7 attenuates BLM-induced lung fibrosis.....	10
<Fig 3> Prodrug BMP-7 attenuates BLM-induced pulmonary fibrosis by downregulating TGF- β /Smad 2/3 pathway	12
<Fig 4> CXCL10, CXCL2/MMP-2, IL-1 β and IL-6 levels in lung tissue lysates and BALF fluid.....	14
<Fig 5> Prodrug BMP-7 decrease inflammatory cells in the BALF of BLM induced lung fibrosis mouse model.....	17
<Fig 6> A group of mice with BLM-induced fibrosis was additionally treated with prodrug BMP-7 to further elucidate its effect on ApoE expression.....	20
<Fig 7> ApoE expression and co-expression with macrophage in normal and IPF lung tissues.....	21

ABSTRACT

Prodrug BMP-7 attenuates pulmonary fibrosis through downregulation of bone marrow derived Apo E+ alveolar macrophage

Background Bone morphogenetic protein-7 (BMP-7) antagonizes transforming growth factor- β (TGF- β), which is critically involved in pulmonary fibrosis. This study investigated the ability of prodrug BMP-7, designed as a micelle formulation nanoparticle of BMP-7, to ameliorate pulmonary fibrosis through nasal inhalation in a preclinical bleomycin (BLM)-induced fibrosis mouse model. In addition, the effect on alveolar macrophages (AM) in BALF was examined using single-cell RNA sequencing.

Materials and Methods After successfully demonstrating the delivery of fluorescently labeled prodrug BMP-7 into murine lungs *in vivo*, animal experiments were conducted on 38 mice (C57BL/6J) divided into three groups: control, BLM, and BLM with prodrug BMP-7. The prodrug BMP-7 and vehicle were inhaled nasally at intervals of 72 h for 21 days, respectively. Subsequently, a single-cell RNA sequence was performed on BALF by dividing it into four groups to analyze the role of prodrug BMP-7 on AM: control, prodrug BMP-7 alone, BLM, and BLM with prodrug BMP-7.

Results Compared with the BLM group, BALF inflammatory cells were significantly reduced in the prodrug BMP-7 group, and the inhibition of fibrosis was confirmed by Masson's trichrome staining and the modified Ashcroft lung fibrosis scoring system. In addition, the downregulation of collagen 1, α -SMA, fibronectin, and TGF- β /SMAD signals and a significant decrease in CXCL10 and CXCL2, which are chemokines secreted by AM, were observed. In BALF, the single-cell RNA sequence proportion of Apo E+ macrophages significantly increased in the BLM group and decreased in the prodrug BMP-7 group. In addition, Apo E+ expression increased in the lung tissues of patients with idiopathic pulmonary fibrosis.

Conclusions These findings indicate that prodrug BMP-7 could be an effective therapeutic agent for pulmonary fibrosis through modulation of Apo E+ AM.

Key words : prodrug bmp-7, Apo E+ alveolar macrophage, pulmonary fibrosis

Prodrug BMP-7 attenuates pulmonary fibrosis through downregulation of bone marrow derived Apo E+ alveolar macrophage

1. INTRODUCTION

Idiopathic pulmonary fibrosis (IPF), the most common type of idiopathic interstitial pneumonia, is characterized by an unclear etiology and poor prognosis with a chronic, progressive nature ¹. The activation of myofibroblasts secretes excessive amounts of extracellular matrix (ECM) and fibrous collagen, leading to fibrosis. Leukocyte and macrophage infiltration, followed by fibroblast migration, is also involved in this process ² ³. In addition, epithelial-mesenchymal transition (EMT) occurs, in which transforming growth factor- β (TGF- β) induces the transition of alveolar epithelial cells to myofibroblasts ⁴.

Numerous cells are involved in the fibrotic reaction, including alveolar epithelial cells, fibroblasts, and macrophages. However, macrophages are heterogeneous, and their contribution to fibrosis development is not fully understood. Some studies have recently reported the fibrotic features of M2 macrophages ^{5,6}, which are considered associated with fibrotic remodeling of the heart, kidneys, liver, and lungs ^{7,8}. Among them, alveolar macrophages (AM) are present in the alveoli, participate in lung homeostasis through foreign particle phagocytosis ⁹, and are involved in fibrogenesis ^{10,11}.

TGF- β and bone morphogenic proteins (BMP) play significant roles *via* counter-regulatory mechanisms ¹². TGF- β is widely known as a key fibrogenic cytokine, indicative of myofibroblast differentiation through a signaling pathway with SMAD2/3. It translocates into the nuclear to regulate the mesenchymal-type genes involved in EMT ^{4,13,14}. In contrast, bone morphogenetic protein-7 (BMP-7) antagonizes TGF- β . Previous studies have

demonstrated that recombinant BMP-7 (rhBMP-7) reversed the TGF- β -induced EMT in pulmonary fibrosis in *in vivo* and *in vitro* models ¹⁵⁻¹⁹.

However, an excess dose with initial burst release of rhBMP is inevitably needed to achieve the clinical efficacy of antifibrosis with rhBMP, which causes unwanted side effects ²⁰. Animal studies have revealed that current soluble rhBMPs exhibit only a half-life of 7–16 min because of rapid elimination and enzymatic degradation ²¹. To overcome the intrinsic limitations of the exogenously introduced soluble growth factor, we developed a prodrug BMP-7 that shows endogenous protein processing to produce active BMP-7, fused with the protein transduction domain (PTD) ²². However, PTD-mediated cellular delivery has pharmacological limitations because of the cargo size (<10 Kd) ²³. Therefore, we developed prodrug BMP-7 of micellized nanoparticles targeting AM, a key regulator of alveolar inflammation. In addition, we investigated its ability to ameliorate pulmonary fibrosis in a preclinical bleomycin (BLM)-induced lung fibrosis mouse model. The effect of prodrug BMP-7 on AM was analyzed using single-cell transcriptomes of BALF cells. Finally, we investigated ApoE expression in IPF human lung tissues.

2. MATERIALS AND METHODS

2.1. Preparation of prodrug BMP-7

The bacterial expression cassette for the prodrug BMP-7 polypeptide and the purification procedures have been previously described ²². Polypeptides were denatured and micellized with filtered 0.1% egg lecithin (BOC Sciences, Shirley, NY, USA) *via* sonication. The typical micelle size, as determined by direct light scattering, was approximately 180–200 nm. The endocytic transduction and exosomal secretion of active BMP-7 have been well established, as described in a previous study ^{24,25}.

2.2. *In vivo* distribution analysis

C57BL/6 mice were intranasally instilled with indocyanine green (ICG)-labeled micellized

prodrug BMP-7 (10 μg) and subjected to *in vivo* fluorescent imaging at different time points. Fluorescent images were obtained using VISQUE® InVivo Smart (Vieworks, Anyang, South Korea) and measured at different time points: 30 min, 1 h, 6 h, 24 h, 48 h, and up to 72 h *in vivo*. In the *ex vivo* experiment, sacrifice was performed on day 7 after inhalation of prodrug BMP-7 (1 μg), and ICG-labeled prodrug BMP-7 contained in the lung tissue was analyzed. All imaging data were analyzed using CleVue™ software (Vieworks).

2.3. Experimental groups

Eight-week-old male C57BL/6 mice weighing 22–25 g were purchased from Orient Bio (Sunnam, Republic of Korea). Mice were supplied with food and water on a 12 h cycle. Thirty-eight mice were divided into three groups: (A) phosphate-buffered saline (PBS) inhalation and vehicle group (control group) ($n = 12$), (B) BLM inhalation and vehicle group (BLM group) ($n = 13$), and (C) BLM-induced pulmonary fibrosis group with prodrug BMP-7 inhalation (BLM + prodrug BMP-7 group) ($n = 13$).

In the control group, 50 μl of sterilized PBS was instilled intranasally. In the other groups, BLM (Sigma, St Louis, MO, USA) 3 U/kg dissolved in 50 μl of PBS was administered similarly. Mice were anesthetized using isoflurane inhalation (Abbott Laboratories) in a supine position *via* microsyringe (Hamilton Company Cat. # 7637-01) with intranasal instillation. The release rate was adjusted so that the mouse could inhale the solution without forming bubbles, similar to the method proposed by Leem et al.²⁶ As post-treatment, prodrug BMP-7 (1.0 $\mu\text{g/g}$ dissolved in 50 μl) or vehicle was inhaled intranasally three times weekly for 3 weeks.

2.4. Method of Experiments

2.4.1. Isolation of bronchoalveolar lavage cells and cell counts

All mice were euthanized 21 days after BLM/PBS injection, and BALF was collected through a tracheal cannula with two 1 ml aliquots of sterile saline. Samples were centrifuged for 10 min at 1,500–5,000 rpm and 4°C. Subsequently, the cell pellet was resuspended in 100 μL of PBS, and cell counting was quantitatively and qualitatively analyzed using a hemocytometer (Marienfeld, Germany). The slides were retrieved,

desiccated, and stained by immersion in Diff-Quick (Sysmex Corporation). The protein content of the BAL supernatant was estimated using Coomassie Brilliant Blue G-250 (Quick Start™ Bradford Protein Assay), and the absorbance was read at 562 nm using a spectrophotometer (specific experimental details are covered in the supplementary document).

2.4.2. Lung tissue harvest and histologic examination

Before protein extraction, the right lung was stored at -80°C after flushing the pulmonary vasculature with saline. The left lung was inflated with low-melting-point agarose (4%) in PBS at 25 cm H_2O pressure until the edges of the pleura became sharp. Subsequently, the tissues were sliced, fixed for 24 h in 10% formaldehyde in PBS, embedded in paraffin, and sectioned at 5 μm . Slides were stained with hematoxylin and eosin (H&E) and Masson's trichrome. Moreover, two qualified investigators evaluated pulmonary fibrosis semiquantitatively according to the modified Ashcroft score scale using a score of 0–8²⁷. In every area, pulmonary fibrosis was recorded as dominant when it occupied >50% of the fields. The final score was presented as the mean of the particular scores observed on all fields.

2.4.3. Western blotting

The frozen lungs were automatically homogenized in 600 μL of homogenization buffer (PRO-PREP™ Extraction Solution), and cell lysis was induced by incubation for 20 min at -20°C . The samples were then centrifuged at 4°C , $13,000 \times g$ for 30 min. The antibodies used in this study included α -SMA (Abcam #ab7817, 1:2,000), collagen I (Abcam #ab34710, 1:2,000), fibronectin (Abcam #ab2413, 1:2,000), β -actin (Santa Cruz #sc-47778, 1:1,000), p-smad2/3 (cell signaling #8828, 1:500), and Smad2/3 (cell signaling #3102, 1:500) (specific experimental details are covered in the supplementary document).

2.4.4. ELISA

The levels of C-X-C motif chemokine 10 (CXCL10), C-X-C motif chemokine 2/matrix metalloproteinase-2 (CXCL2/MMP-2), interleukin-1 β (IL-1 β), and interleukin 6 (IL-6) in whole-lung homogenates and BAL fluid were measured using quantified ELISA kits (Cat

No. RND-LXSAMSM-05_Mouse Premixed Multi-Analyte Kit) according to the manufacturer's instructions. The cytokines used in this study included CXCL10, CXCL2/MMP-2, IL-1 β , and IL-6 (R&D Systems).

2.4.5. Single cell RNA-seq analysis of BALF cells

BALF single-cell RNA sequencing (scRNA-seq) analysis was conducted in four groups. Eighteen mice were divided into four groups with the addition of the prodrug BMP-7-alone group: PBS group (control group) ($n = 6$) (G1), prodrug BMP-7 group ($n = 6$) (G2), BLM group ($n = 3$) (G3), and BLM + prodrug BMP-7 ($n = 3$) (G4).

BALF single cells were collected and pooled for each group. In total, 40,000 cells per group were loaded onto microwell cartridges of the BD Rhapsody Express system (BD). Single-cell whole transcriptome analysis libraries were prepared using BD Rhapsody WTA Reagent Kit (BD: 633802) according to the manufacturer's instructions. The final index PCR libraries were sequenced on Illumina HiSeq using High Output Kit v2.5 (150 cycles, Illumina) for 2×75 bp paired-end reads with an 8 bp single index.

The FASTQ-format sequencing raw data were processed through the BD Rhapsody WTA Analysis pipeline (version 1.0, Revision 6) on the SevenBridges Genomics online platform (SevenBridges). Expression matrix was used for further data analysis. Unless otherwise specified, data normalization, dimensionality reduction, and visualization were performed using the Seurat package (version 4.3.0). Cells were filtered based on the following criteria to ensure data quality: having 500–6,000 genes per cell (nFeature_RNA) and a percentage of mitochondrial genes (percent.mito) of <25. For the unsupervised hierarchical clustering analysis, the FindClusters function in the Seurat package was implemented. Various resolutions of 0.1–0.9 were tested, and the final resolution was selected based on the most stable and relevant outcome, utilizing the clustree R package and considering prior knowledge (specific experimental details are covered in the supplementary document).

2.4.6. Immunofluorescence & Immunohistochemistry staining

ApoE recombinant rabbit monoclonal (Thermo Fisher Scientific, Catalog No. 701241) and the macrophage marker, CD68 (Santa Cruz Biotherapy, Inc., Catalog No. sc-20060), were

diluted in DAKO antibody dilution buffer (1:1,000) and cultivated overnight at 4°C. Goat anti-rabbit IgG secondary antibody, Alexa Fluor™ 488, or goat anti-mouse IgG secondary antibody, Alexa Fluor™ 568 (Invitrogen), was diluted 1:1,000 and cultivated for 1 h at room temperature. After washing the secondary antibodies with PBS, nuclei were stained for 20 min with 1 µg/ml DAPI.

Fluorescence images were obtained using a Zeiss LSM700 confocal microscope (Carl Zeiss, Berlin, Germany). Morphological analysis of the confocal images was performed using Metamorph microscopy analysis software (version 7.1, Molecular Devices, Sunnyvale, CA, USA).

2.5. Statistics

Data were compared using unpaired Student's *t*-test or ANOVA with Bonferroni's multiple comparisons in Prism 5.0 (GraphPad Software, Durham, NC, USA). Data were reported as mean ± SD, and differences were considered significant at $P < 0.05$.

2.6. Study approval

Animal protocols were approved by the Institutional Animal Care Committee, Yonsei University College of Medicine (2021-31-0820). They followed the recommendations of the Guide for the Care and Use of Laboratory Animals by the National Institutes of Health. The human study population comprised paraffin-embedded lung tissue samples collected from two patients with IPF and one normal control diagnosed with pneumothorax. Case 1: A 61-year-old male patient diagnosed with IPF underwent left lung transplantation in August 2022. Case 2: A 56-year-old male patient diagnosed with IPF underwent left lung transplantation in August 2022. The normal control group included a patient who underwent thoracic surgery for pneumothorax. The study protocols were approved by the Institutional Review Board of Severance Hospital (Approval no. 4-2013-0770 IPF patient's registry, 4-2019-0447 normal lung registry group). This study adhered to the principles of the Declaration of Helsinki (2000) and the Declaration of Istanbul (2008).

3. RESULTS

3.1. Prodrug BMP-7 is delivered to the alveoli and shows prolonged tissue retention

To determine whether the inhaled prodrug BMP-7 is delivered to the small airways and alveoli and retained in pulmonary tissue, we performed a lung distribution dosing study in an *in vivo* and *ex vivo* mouse model. Nine C57BL/6 mice were intranasally instilled with ICG-labeled prodrug BMP-7 (1 and 10 μg) and imaged using the IVIS system at different time points: 30 min, 1 h, 6 h, 24 h, 48 h, and up to 72 h *in vivo*. The inhaled prodrug BMP-7 was retained in the lung tissue for up to 72 h at a dose of 10 μg (Figure 1A). Figure 1B shows an experiment with different concentrations (1 and 10 μg). The drug reached its maximum level within the first hour after inhalation and remained in the lung tissue for approximately 48 h for the prodrug BMP-7 1 μg group ($n = 9$) and 72 h for the 10 μg group ($n = 9$). Higher drug concentration results in higher radiation intensity and longer duration. Furthermore, in the *ex vivo* prodrug BMP-7 distribution analysis, an autopsy was performed on day 7 after inhalation administration of 1 μg of prodrug BMP-7. The remaining drug in the lung tissue was analyzed using IVIS. Prodrug BMP-7 remained in the lung tissue even after 1 week of nasal inhalation compared with the control group (Figure 1C and D). In addition to the results of *in vivo* and *ex vivo* distribution analysis, the effective drug concentration and the number of inhalations were determined to be 1 μg and repeated instillation within 72 h, respectively. Moreover, immunofluorescence staining was performed 24 h later in the mouse group that inhaled the nanoparticle prodrug BMP-7; through this, it was confirmed that the prodrug BMP-7 was delivered to the alveoli and small airway *via* inhalation (Supplementary Figure 1).

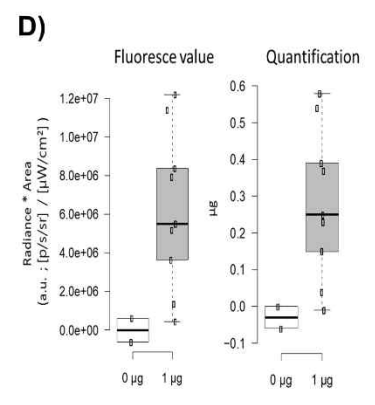
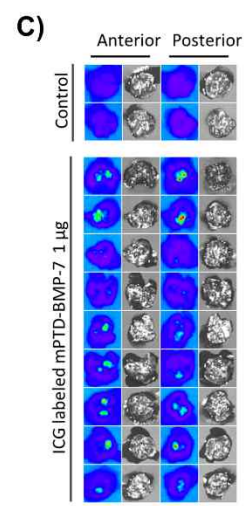
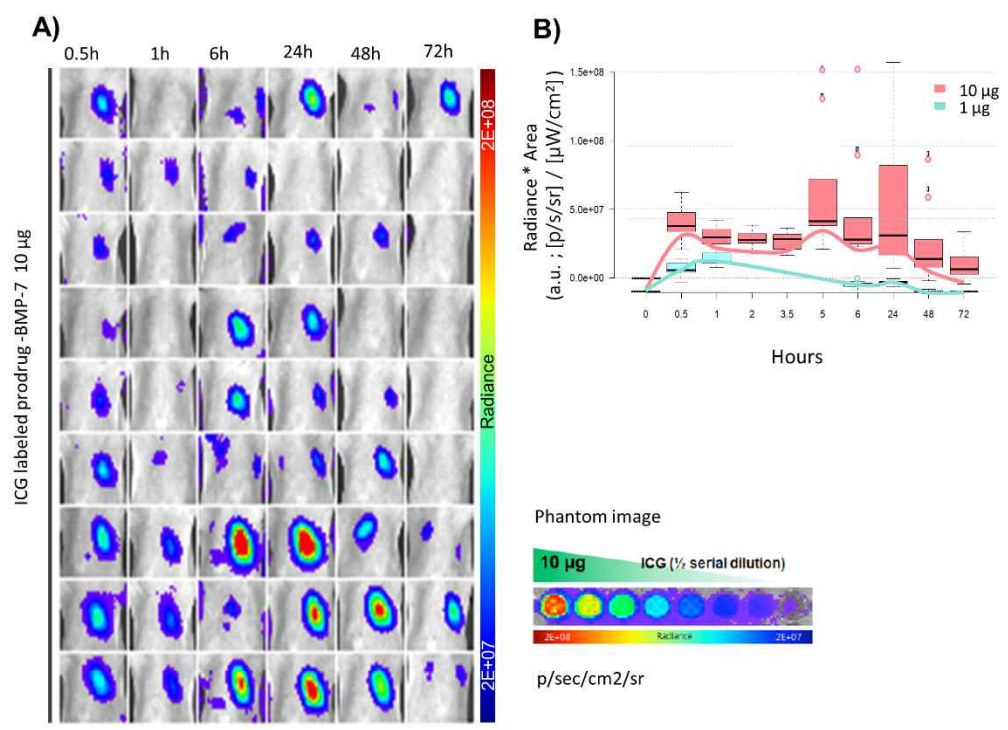


Figure 1. *In vivo* IVIS imaging. (A) *In vivo* IVIS images of C57BL/6 mice with intranasal instillation of prodrug BMP-7 (10 µg). (B) Inhalation of different concentrations of prodrug BMP-7 with 1 and 10 µg, respectively, within 72 h. (C) *Ex vivo* experiment with ICG-labeled prodrug BMP-7 (1 µg) after 7 days of inhalation exposure. (D) Comparison of fluorescence values and radiation quantification between the control and experimental groups (prodrug BMP-7, 1 µg inhalation)

3.2. Prodrug BMP-7 attenuates BLM-induced pulmonary fibrosis

Figures 2A and B show that BLM induced inflammatory cell infiltration, increasing total BALF cells, in contrast inhaled prodrug BMP-7 decreased BALF inflammatory cell and total cell counts (29.25×10^4 in the control group, 504.00×10^4 in the BLM group, and 105.00×10^4 in the prodrug BMP-7 group; $P < 0.001$). In addition, Figure 2C shows that histological changes related to pulmonary fibrosis were observed in H&E and Masson's trichrome staining. Lung tissue exposed to PBS was well organized and free of inflammatory cells and collagen deposits in the alveoli. BLM-exposed tissues showed disordered structures, thickened interalveolar septa, inflammatory cell infiltration, and collagen deposits in the interstitium. In contrast, inhaled prodrug BMP-7 decreased collagen matrix density, as shown by Masson's trichrome staining and quantitatively measurement of total collagen content using ImageJ. Moreover, the modified Ashcroft lung fibrosis score was augmented in the BLM group compared with the control group, and prodrug BMP-7 inhalation improved the fibrosis score (0.00 in the control group, 5.00 in the BLM group, and 3.00 in the inhaled prodrug BMP-7 group; $P < 0.001$) (Figure 2D).

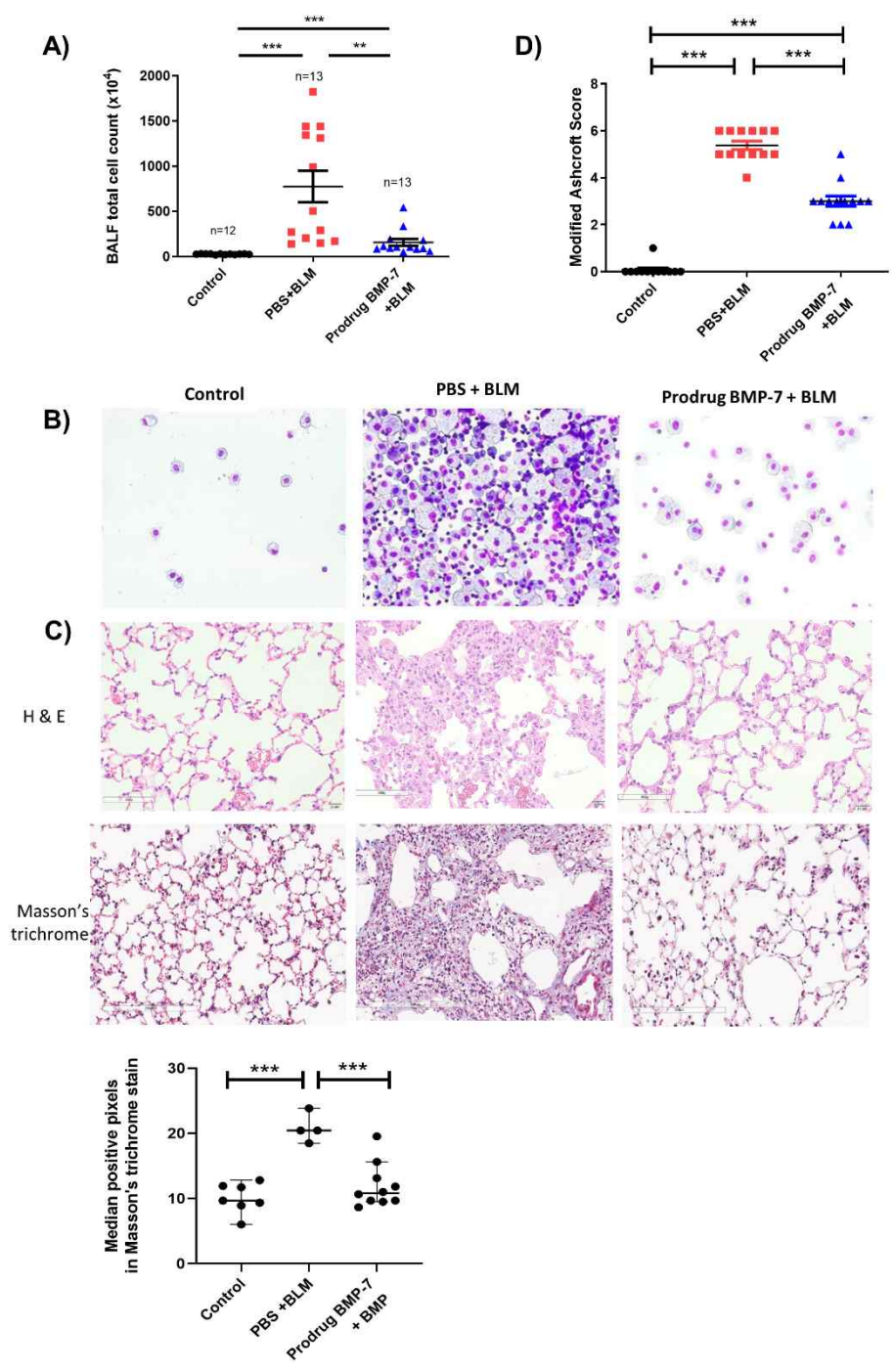


Figure 2. Inhaled prodrug BMP-7 attenuates BLM-induced lung fibrosis (A) Cell counts and (B) cytology in BALF (C) Lung tissues stained with H&E and Masson's trichrome stain, magnification 200x, total collagen count measured by ImageJ pixels. (D) Modified Ashcroft lung fibrosis scores in mice lung tissue. Micellized prodrug BMP-7 decreased inflammatory cells, fibrotic lesions, and modified Ashcroft lung fibrosis score compared with those in the BLM group. * $P < 0.05$; ** $P < 0.01$; and *** $P < 0.001$.

3.3. Prodrug BMP -7 inhibits the TGF- β /Smad2/3 signaling pathway in BLM-induced pulmonary fibrosis.

The antifibrotic effect of prodrug BMP-7 was characterized by a lower level of ECM proteins represented as fibrosis markers, such as collagen I, fibronectin, and α -SMA compared with the BLM group ($P < 0.05$; Figure 3A–D). Given the antifibrotic effect of prodrug BMP-7, we determined whether the mechanism involves the downregulation of TGF- β /Smad 2/3 signaling. Therefore, the expression of TGF- β /Smad 2/3 signaling was measured in all groups. As measured by Western blotting on day 21, BLM stimulated the expression of phosphorylation of Smad 2/3 relative to the control group. Prodrug BMP-7 inhalation attenuated the expression of phosphorylation of Smad 2/3 ($P < 0.001$; Figure 3E). These results revealed that prodrug BMP-7 attenuated pulmonary fibrosis by downregulating TGF- β /Smad 2/3 signaling.

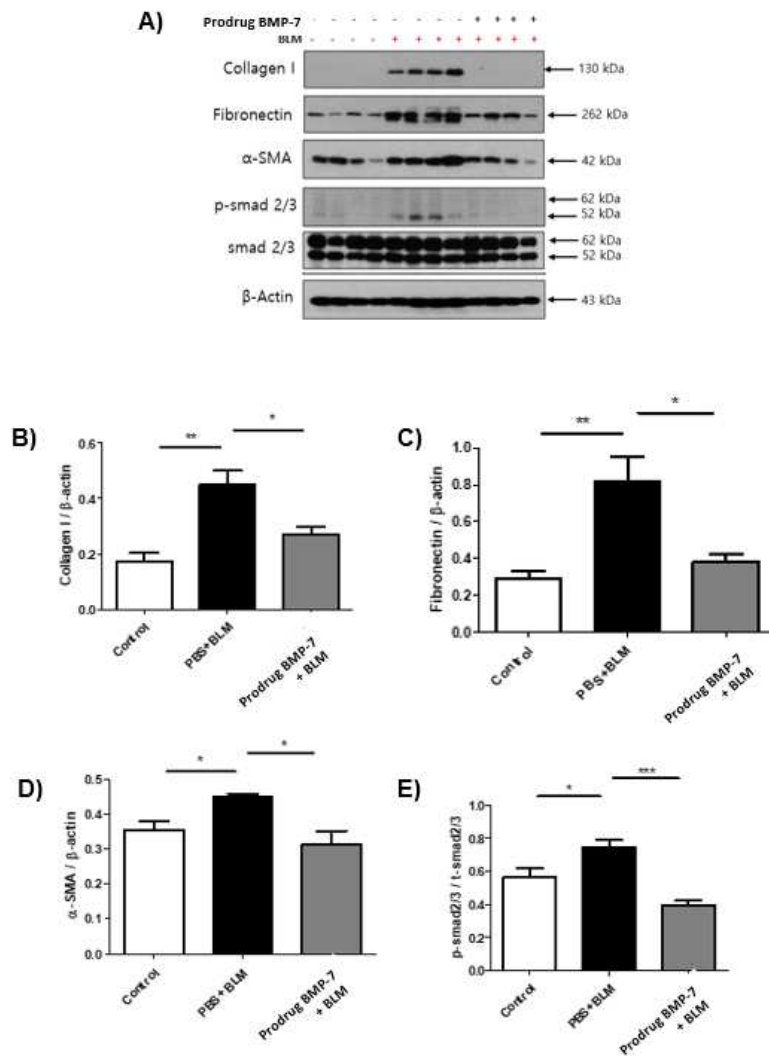


Figure 3. Prodrug BMP-7 attenuates BLM-induced pulmonary fibrosis by downregulating TGF- β /Smad 2/3 pathway. Fibrosis markers and Smad protein were detected using Western blotting in mouse lung tissue to assess the antifibrosis effect of prodrug BMP-7 (Figure 3A). Prodrug BMP-7 suppressed the expression of collagen I (3B), fibronectin (3C), α -SMA (3D), and p-Smad 2/3 (3E). The data represent the means

± SD. * $P < 0.05$; ** $P < 0.01$; and *** $P < 0.001$.

3.4. Prodrug BMP-7 attenuates BLM-induced pulmonary fibrosis by suppressing CXCL10, CXCL2/MIP-2, IL-1 β and IL-6

To determine the antifibrosis effect of prodrug BMP-7, we evaluated the levels of CXCL10, CXCL2/MIP-2, IL-1 β , and IL-6 using ELISA on day 21 with mouse lung tissue lysates. CXCL10, CXCL2/MIP-2, IL-1 β , and IL-6 levels significantly increased after exposure to BLM. However, these levels decreased after inhalation of prodrug BMP-7 (Figure 4A–D). The same result was observed in BALF (Figure 4E and F).

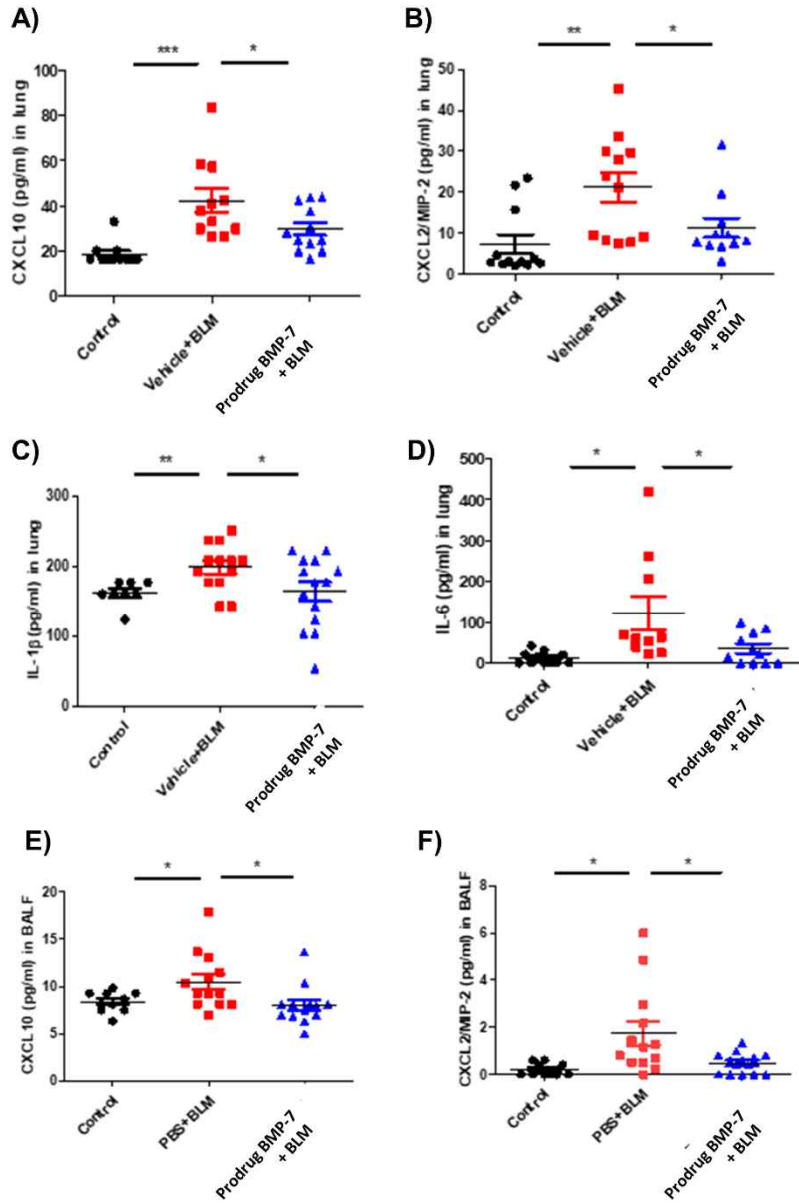


Figure 4. CXCL10, CXCL2/MMP-2, IL-1 β , and IL-6 levels in lung tissue lysates and BALF fluid. Cytokine levels measured using ELISA decreased in mice with prodrug BMP-7 inhalation compared with those in the BLM-induced lung injury group. CXCL10,

CXCL2/MMP-2, IL-1 β , and IL-6 (A–D) in lung tissue lysates (E–F) of BALF. Values are presented as means \pm SD * $P < 0.05$; ** $P < 0.01$; and *** $P < 0.001$.

3.5. Prodrug BMP-7 changes the composition of inflammatory cells in the BALF of BLM- induced lung fibrosis mouse model

The BLM-induced lung fibrosis mouse model was divided into four groups: the PBS group (control group) (G1), the prodrug BMP-7 group (G2), the BLM group (G3), and the BLM + prodrug BMP-7 (G4) (Figure 5A). scRNA-seq was performed using the BD Rhapsody platform. After removing doublets, 97,219 filtered cells were analyzed using the algorithm of uniform manifold approximation and projection (UMAP). Each cluster was identified using representative marker genes for each cell type (Figure 5B and Supplementary Figure 2). The proportion of each cell type demonstrated differences between groups (Figure 5C). Notably, the proportion of macrophages decreased in the BLM treatment group (G3) compared with the control groups (G1 and G2). However, it exhibited an increase in the BLM+ prodrug BMP-7 treatment group (G4) compared with G3; the proportion of T/NK cells changed reciprocally.

Conversely, no significant difference was observed between the prodrug BMP-7 group (G2) and the control group (G1).

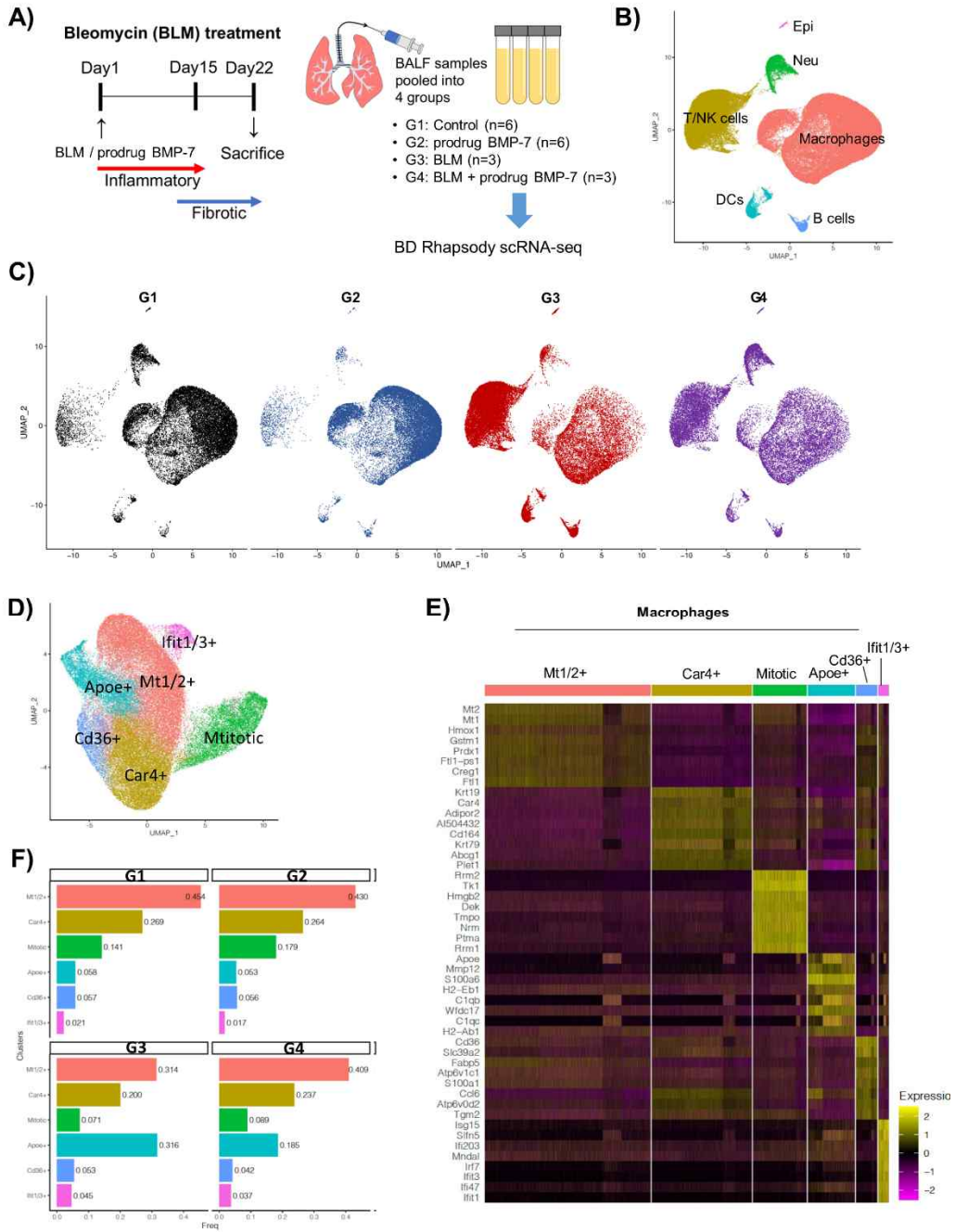
Cells designated as macrophages were isolated for subpopulation analysis to explore the role of macrophages in BLM-induced lung fibrosis (Figure 5D). A total of 57,293 macrophages were divided into six subclusters, each subcluster named using one of the top eight differentially expressed genes (DEGs) (Figure 5E): Mt1/2+ macrophages, Car4+ macrophages, mitotic macrophages, Apo E+ macrophages, Cd36+ macrophages, and Ifit1/3+ macrophages.

Compared with the control groups (G1 and G2), the proportion of Apo E+ macrophages significantly increased in the BLM treatment group (G3) and decreased in the prodrug BMP-7 and BLM treatment group (G4) (Figure 5F).

When plotting a volcano plot using DEGs, G3 *versus* G1 and G4 *versus* G3 showed a mirror-like pattern (Supplementary Figure 3). Fewer DEGs were observed in G2 *versus* G1, G4 *versus* G1, and G4 *versus* G2. In addition, violin plots of genes differentially expressed in G1, G3, and G4 are shown (Supplementary Figure 4). In each subcluster, the genes ApoE, C1qb, and H2-Eb1 increased in G3 compared with the control groups (G1, G2) and subsequently decreased in G4. However, the genes Mt1 and Mt2 showed an opposite pattern, decreasing in G3 and increasing in G4.

Apo E⁺ macrophages, which exhibited high average Cd14, ApoE, Mafk, and Ccr2 expression levels, were designated bone marrow-derived macrophages (BMM). The remaining macrophage subtypes, excluding mitotic macrophages and Ifit1/3⁺ macrophages, namely, Mt1/2⁺ macrophages, Car4⁺ macrophages, and Cd36⁺ macrophages, were combined as resident macrophages (ResM). Trends of increase and decrease in DEGs were observed (Figure 5G). ApoE and C1qb in ResM and BMM increased in G3 compared with the control groups (G1, G2) and then decreased in G4. The pattern for H2-Eb1 in ResM was similar to that in ApoE and C1qb. However, in BMM, it increased in G3 compared with G1 and then decreased in G4. For Mt1 in ResM and Mt2 in ResM and BMM, a decrease in G3 was observed, followed by an increase in G4, whereas Mt1 in BMM decreased in G3 with little change observed in G4 (Figure 5H and Supplementary Figure 5).

Gene set enrichment analysis (GSEA) was performed using DEGs between G1 and G3 and G3 and G4 in ResM and BMM. The top 10 and bottom 10 enriched pathways were identified based on the normalized enrichment score values (Supplementary Figures 6 and 7). In G3, genes related to the coagulation and complement pathways increased, whereas they decreased in G4.



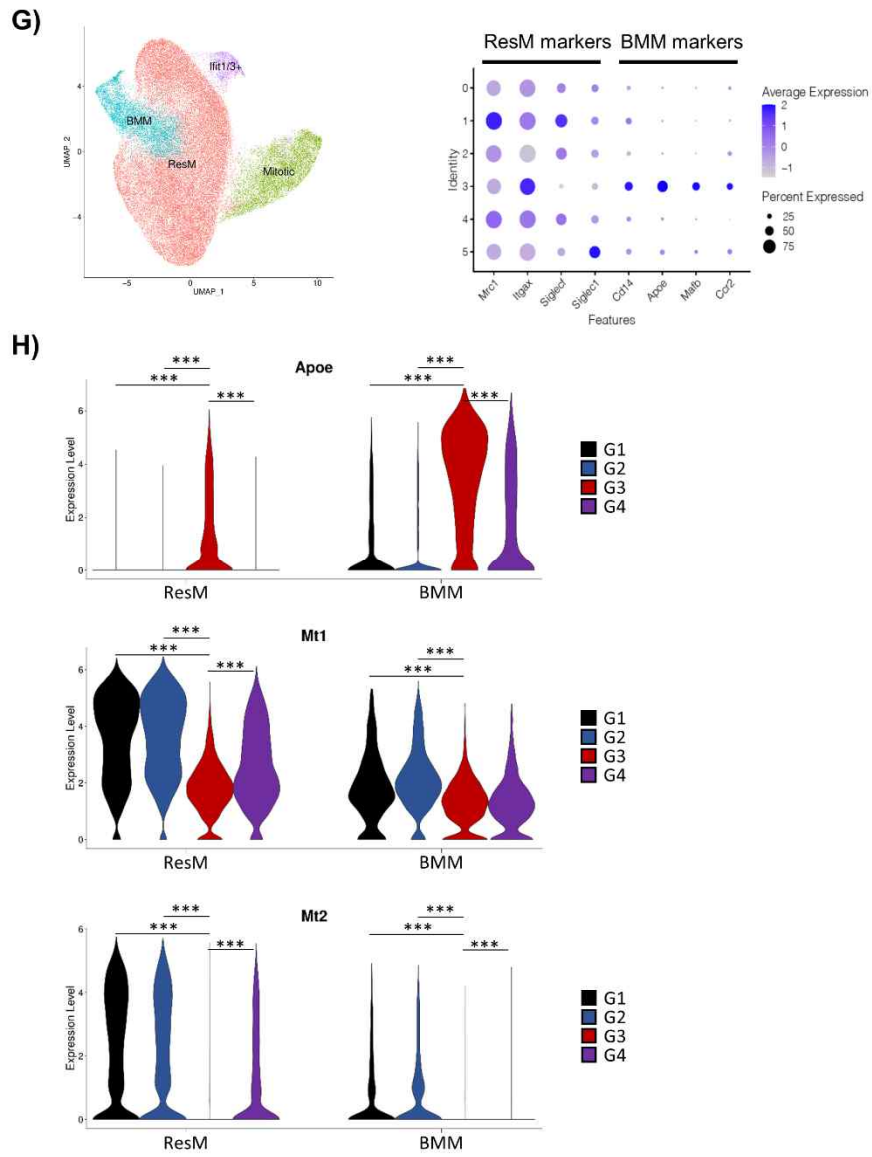


Figure 5. Prodrug BMP-7 decrease inflammatory cells in the BALF of BLM induced lung fibrosis mouse model. (A) Schematic of experimental design for single-cell transcriptomes of BALF cells. (B) Cell-type annotations projected into UMAP space.

(C) UMAP colored for and separated by control (black), prodrug BMP-7 (dark blue), BLM (red), and BLM with prodrug BMP-7 (purple) of BALF scRNA-seq data. (D) UMAP visualization of macrophage subclusters. (E) Heatmap of top marker genes for macrophages with normalized expression colorized (low expression, purple; high expression, yellow). (F) Bar plots of the proportion of macrophage subclusters in each group. (G) UMAP plot of reclassified macrophage subclusters using ResM and BMM markers. (H) Violin plots of ApoE, Mt1, and Mt2 gene expression in ResM and BMM across each group.

3.6. Prodrug BMP-7 changes ApoE expression with macrophages in a BLM-induced fibrosis mouse model and normal and IPF human lung tissues

Immunofluorescence and immunohistochemistry staining were performed to evaluate the role of prodrug BMP-7 in ApoE expression on AM. Figure 6A shows that exclusive expression of macrophages was observed in mice treated with the prodrug BMP-7 vehicle. The BLM group exhibited increased ApoE expression within the cytoplasm of AM (Figure 6B), and the prodrug BMP-7 group showed a marked decrease in ApoE expression on AM (Figure 6C), indicating possible downregulation of ApoE expression in response to prodrug BMP-7. Furthermore, the response of ApoE expression to AM in normal and IPF human lung tissues was investigated. Figure 7A and B show that, in the patient's normal lung tissue, ApoE immunostaining showed the absence of cytoplasmic ApoE expression. In addition, the bronchioles showed exclusive expression of macrophages with no detectable cytoplasmic ApoE expression (Figure 7C and D). However, in the patient with IPF lung tissue, ApoE immunostaining showed robust and active ApoE expression, observed in the bronchioles or alveolar sacs and within the interstitium (Figure 7E–J). The patient with IPF in case 1 (Figure 7E and F) was a 3.3-pack-year ex-smoker. Histology exhibited marked fibrosis with fibroblastic foci, airway dilatation, and moderate inflammation, consistent with the pathological findings of usual interstitial pneumonia. The patient with IPF in case 2 (Figure 7I and J) was a 75-pack-year ex-smoker with emphysema and IPF. Pathology

revealed marked fibrosis and moderate inflammation with emphysema-like bullae and fibroblastic foci. Immunofluorescence staining was performed to elucidate the functional role of ApoE. In addition, it explored the intricate interplay of cells and proteins in the gas exchange region and its involvement in inflammatory and immune responses with macrophages. The analysis revealed strong ApoE expression in the cytoplasm surrounding the nucleus, colocalizing with the presence of macrophages, which indicates that ApoE expression is induced and promoted in human pulmonary fibrosis.

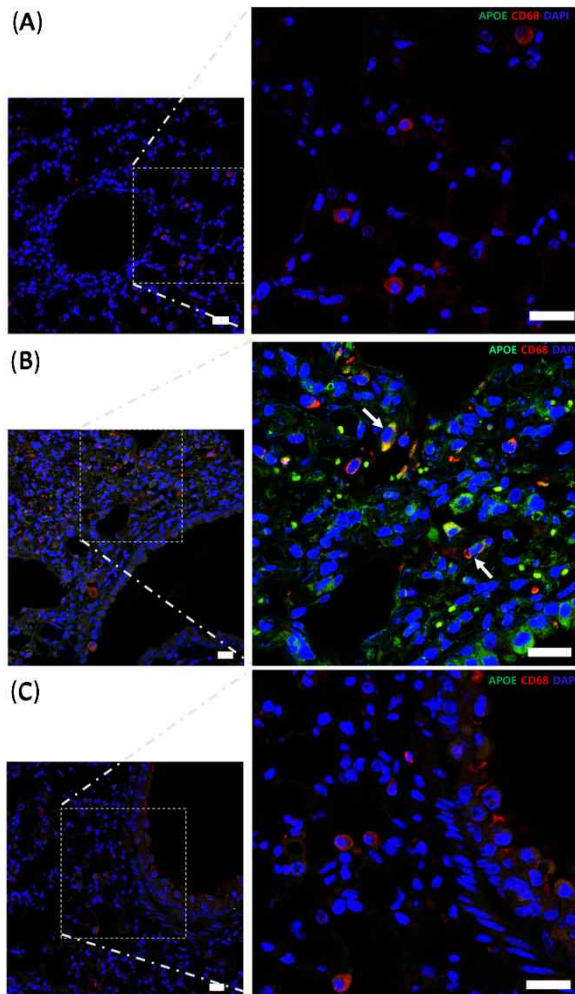


Figure 6. A group of mice with BLM-induced fibrosis was further treated with prodrug BMP-7 to determine its effect on ApoE expression.

(A) In the group of mice treated with the vehicle of the prodrug BMP-7, exclusive expression of macrophages was observed (shown in green). (B) In the group of mice treated with BLM alone, cells co-expressing ApoE with macrophages exhibited cytoplasmic localization (highlighted by white arrows), accompanied by a significant increase in ApoE expression within the cytoplasm (shown in red). (C) In a group of mice treated with prodrug BMP-7 in combination with BLM, a distinct pattern was observed. ApoE expression was markedly decreased in the treated group, except for certain cells, particularly macrophages (shown by green fluorescence), indicating a possible downregulation of ApoE expression in response to prodrug BMP-7 in the presence of BLM-induced fibrosis. Cell nuclei were counterstained with DAPI (blue); scale bar: 20 μ m

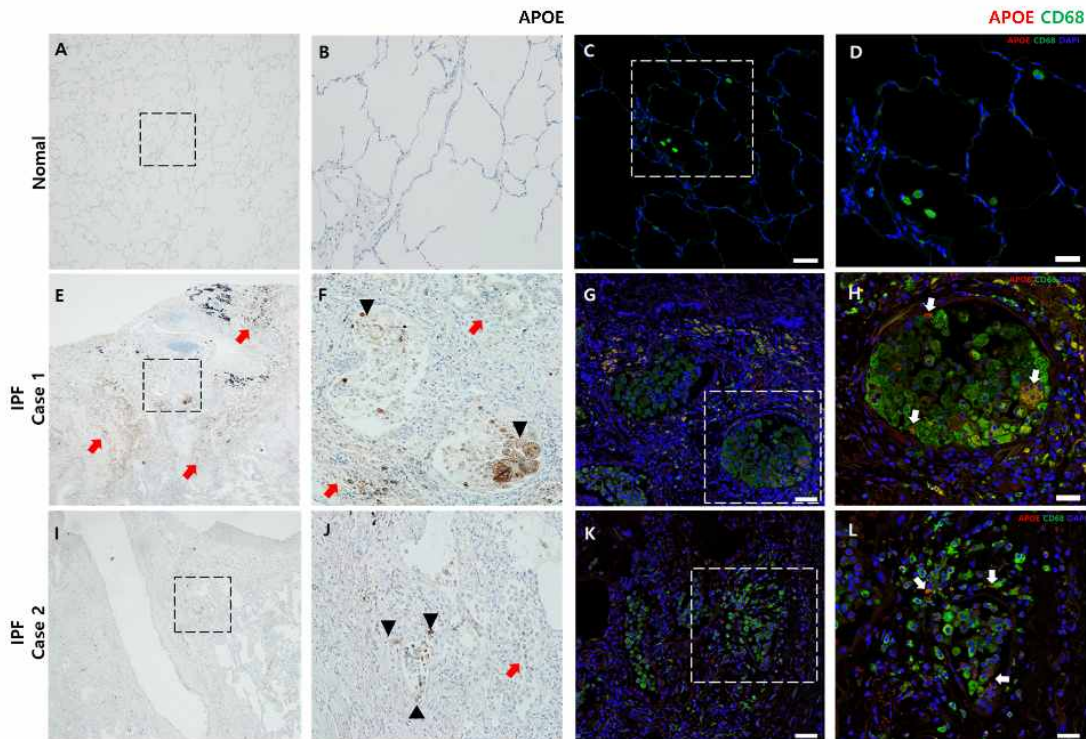


Figure 7. ApoE expression and co-expression with macrophage in normal and IPF lung tissues. (A, B) In the normal lung tissue, ApoE immunostaining revealed the absence of cytoplasmic ApoE expression. ApoE was not detected in the cellular cytoplasm after immunostaining. (C, D) Within the normal lung tissue, bronchioles showed exclusive expression of macrophages (shown in green) with no detectable cytoplasmic ApoE expression. (E, F, I, J) In contrast, in the IPF lung tissue of the patient, ApoE immunostaining exhibited robust and active ApoE expression, observed in the bronchioles or alveolar sacs (shown as black spots) and within the interstitium (red arrows). (G, H, K, L) Immunofluorescence staining was performed to elucidate the functional role of ApoE in the pathway from bronchioles to lung tissue and explore the intricate interplay of cells and proteins in the gas exchange region, as well as its involvement in inflammatory and immune responses with macrophages. The analysis revealed strong ApoE expression (shown in red) in the cytoplasm surrounding the nucleus (blue), colocalizing with the presence of macrophages (shown in green). Cell nuclei were counterstained with DAPI (blue); scale bar: 20 μ m.

4. DISCUSSION

In this study, we developed the micellized nanoparticle prodrug BMP-7, targeting AM, a primary regulator of the alveolar immune response. The pulmonary antifibrotic effect was demonstrated in a murine bleomycin model. Recent studies have reported that two ontological populations of AM co-exist during pulmonary fibrosis: ResM and BMM²⁸⁻³⁰. Therefore, we hypothesized that there would be subtypic changes occur in AM after prodrug BMP-7 inhalation. In addition, after analyzing scRNA-seq using BALF, downregulation of ApoE AM was remarkably identified among the other six subclusters, and immunostaining of IPF patients confirmed the upregulation of ApoE and colocalized macrophages. These data indicate that the prodrug BMP-7 could have a potential antifibrotic effect by downregulating bone marrow-derived Apo E+ AM.

Few studies have investigated the role of bone marrow-derived Apo E+ AM during fibrosis. Cui *et al.* reported that pulmonary ApoE was produced almost exclusively by BMM in mice with BLM-induced lung fibrosis and directly bound to collagen I, which mediated phagocytosis in a low-density lipoprotein receptor (LDLR) dependent manner³¹. Furthermore, ApoE-knockout mice administered with ApoE protein exhibited a resolution of lung fibrosis. This study revealed that although ApoE is not essential for the development of fibrosis, it plays a crucial role in the resolution of BLM-induced fibrosis.

In contrast, some studies have reported that disrupted lipid metabolism in the alveolar microenvironment is more affectable to pulmonary fibrosis than specific lipid protein, such as LDL or Apo E^{32,33}. Shi *et al.* demonstrated higher LDL protein induced cell apoptosis and TGF- β production in an *in vitro* experiment, and showing LDLR knockout mice induced fibroblast-like cell accumulation inducing pulmonary fibrosis³⁴.

The primary function of macrophages is innate immunity; alternative functions include lipid metabolism. The M1 and M2 phenotypes are known to be programmed through different metabolic pathways performed by free fatty acid oxidation and free fatty acid synthesis²⁹. Lipid metabolic imbalance is known to be associated with the macrophage process, which promotes fibrosis^{31,35,36}. Inflammatory signals, including LPS and IFN γ , required to generate the M1 phenotype induce fatty acid synthesis³⁷. However, the inhibition of inflammatory signals required for M2 macrophage differentiation involves fatty acid oxidation³⁸.

After bleomycin injury, some subtypes of AM undergo fatty acid oxidation and are transformed into the M2 phenotype, and the bone marrow derived Apo E+ subtype in this study shows similar findings. In addition, a decrease in resident AM, such as M α 1/2+ is also seen, which is indicating that macrophages respond differently to lung injury with distinct functional features. This finding is consistent with reports in analyses of BMM subgroups using single-cell sequencing that different groups act differently, such as in the regulation of leukocyte or lymphocyte migration.³⁹ Taken together, inhalation of the prodrug BMP-7 probably downregulates Apo E + AM, one of the subgroups of AMs, restores homeostasis of lipid metabolism, and reduces cell death and pro-inflammatory responses.

Subsequently, it reduces fibroblast attractants CXCL10 and CXCL2 and may be associated with inhibition or resolution of fibrosis.

In BMM and ResM, compared with G1, the hallmark of coagulation and complement pathway was detected within the top 10 in G3. In addition, compared to G3, it was detected within the bottom 10 in G4 (Supplementary Figures 6 and 7). The decrease in Mt1 and Mt2 genes in G3, in which fibrosis was induced, compared with the control groups (G1, G2), and their subsequent increase from G3 to G4 is consistent with previous research findings that fibrosis increases in the hearts of Mt1/2 knockout mice⁴⁰. The decrease in G3, in which fibrosis was induced, and the increase in G4 agree with previous research findings. Mt1 has various immunomodulatory effects by modulating several signal transduction pathways, such as phosphorylation of STAT signaling pathways and NF- κ B signaling⁴¹. However, the role of Mt1/2 during fibrosis has been rarely reported. It is known to be associated with organ remodeling, with published data attenuated myocardial remodeling in Mt-overexpressing mice⁴².

Recent studies have indicated that the complement system plays a significant role in fibrosis^{43,44}. Addis-Lieser et al. reported that C5 knockout mice demonstrate reduced BLM-induced lung injury compared with wild-type mice. C5 also plays a profibrotic role. In this experiment, the C1qb gene increased in G3 and decreased in G4, as reflected in the GSEA results.

In the GSEA for BMM G4 *versus* G3, the hallmark of the TGF- β pathway was detected as the sixth lowest pathway with an adjusted *P*-value of 0.13, indicating its potential relevance despite not being significantly enriched.

5. CONCLUSION

In conclusion, our findings suggest that modulation of lipid homeostasis through AM, particularly Apo E+ AM, could be a therapeutic target for the treatment of pulmonary

fibrosis. In addition, prodrug BMP-7, which modulates Apo E+ AM, could be suitable for this process. Further research is required to determine whether prodrug BMP-7 suppresses inflammation or fibrosis stages, and additional experiments using ApoE-knockout mice are necessary.

REFERENCES

1. Gross TJ, Hunninghake GW. Idiopathic pulmonary fibrosis. *N Engl J Med* 2001;345(7):517-25. doi: 10.1056/NEJMra003200 [published Online First: 2001/08/25]
2. Selman M, Pardo A. Role of epithelial cells in idiopathic pulmonary fibrosis: from innocent targets to serial killers. *Proc Am Thorac Soc* 2006;3(4):364-72. doi: 10.1513/pats.200601-003TK [published Online First: 2006/06/02]
3. Crosby LM, Waters CM. Epithelial repair mechanisms in the lung. *Am J Physiol Lung Cell Mol Physiol* 2010;298(6):L715-31. doi: 10.1152/ajplung.00361.2009 [published Online First: 2010/04/07]
4. Willis BC, Liebler JM, Luby-Phelps K, et al. Induction of epithelial-mesenchymal transition in alveolar epithelial cells by transforming growth factor-beta1: potential role in idiopathic pulmonary fibrosis. *Am J Pathol* 2005;166(5):1321-32. doi: 10.1016/s0002-9440(10)62351-6 [published Online First: 2005/04/28]
5. Lis-López L, Bauset C, Seco-Cervera M, et al. Is the Macrophage Phenotype Determinant for Fibrosis Development? *Biomedicines* 2021;9(12) doi: 10.3390/biomedicines9121747 [published Online First: 2021/12/25]
6. Chen X, Tang J, Shuai W, et al. Macrophage polarization and its role in the pathogenesis of acute lung injury/acute respiratory distress syndrome. *Inflamm Res* 2020;69(9):883-95. doi: 10.1007/s00011-020-01378-2 [published Online First: 2020/07/11]
7. Hashimoto D, Chow A, Noizat C, et al. Tissue-resident macrophages self-maintain locally throughout adult life with minimal contribution from circulating monocytes. *Immunity* 2013;38(4):792-804. doi: 10.1016/j.immuni.2013.04.004 [published Online First: 2013/04/23]
8. Zhang L, Wang Y, Wu G, et al. Macrophages: friend or foe in idiopathic pulmonary fibrosis?

- Respiratory Research* 2018;19(1):170. doi: 10.1186/s12931-018-0864-2
9. Cai Y, Sugimoto C, Arainga M, et al. In Vivo Characterization of Alveolar and Interstitial Lung Macrophages in Rhesus Macaques: Implications for Understanding Lung Disease in Humans. *The Journal of Immunology* 2014;192(6):2821-29. doi: 10.4049/jimmunol.1302269
 10. Joshi N, Walter JM, Misharin AV. Alveolar Macrophages. *Cellular Immunology* 2018;330:86-90. doi: <https://doi.org/10.1016/j.cellimm.2018.01.005>
 11. Philip K, Mills WT, Davies J, et al. HIF1A up-regulates the ADORA2B receptor on alternatively activated macrophages and contributes to pulmonary fibrosis. *The FASEB Journal* 2017;31(11):4745-58. doi: <https://doi.org/10.1096/fj.201700219R>
 12. Lin SJ, Lerch TF, Cook RW, et al. The structural basis of TGF- β , bone morphogenetic protein, and activin ligand binding. *Reproduction* 2006;132(2):179-90. doi: 10.1530/rep.1.01072
 13. Derynck R, Muthusamy BP, Saeteurn KY. Signaling pathway cooperation in TGF- β -induced epithelial-mesenchymal transition. *Current Opinion in Cell Biology* 2014;31:56-66. doi: <https://doi.org/10.1016/j.ceb.2014.09.001>
 14. Gonzalez DM, Medici D. Signaling mechanisms of the epithelial-mesenchymal transition. *Sci Signal* 2014;7(344):re8. doi: 10.1126/scisignal.2005189 [published Online First: 2014/09/25]
 15. Yang G, Zhu Z, Wang Y, et al. Bone morphogenetic protein-7 inhibits silica-induced pulmonary fibrosis in rats. *Toxicol Lett* 2013;220(2):103-8. doi: 10.1016/j.toxlet.2013.04.017 [published Online First: 2013/05/04]
 16. Yang G, Zhu Z, Wang Y, et al. Bone morphogenetic protein 7 attenuates epithelial-mesenchymal transition induced by silica. *Hum Exp Toxicol* 2016;35(1):69-77. doi: 10.1177/0960327115577550 [published Online First: 2015/03/04]
 17. Liang D, Wang Y, Zhu Z, et al. BMP-7 attenuated silica-induced pulmonary fibrosis through modulation of the balance between TGF-beta/Smad and BMP-7/Smad signaling pathway. *Chem Biol Interact* 2016;243:72-81. doi: 10.1016/j.cbi.2015.11.012 [published Online First: 2015/11/21]
 18. Li X, An G, Wang Y, et al. Anti-fibrotic effects of bone morphogenetic protein-7-modified bone marrow mesenchymal stem cells on silica-induced pulmonary fibrosis. *Exp Mol Pathol* 2017;102(1):70-77. doi: 10.1016/j.yexmp.2016.12.010 [published Online First:

2017/01/08]

19. Izumi N, Mizuguchi S, Inagaki Y, et al. BMP-7 opposes TGF-beta1-mediated collagen induction in mouse pulmonary myofibroblasts through Id2. *Am J Physiol Lung Cell Mol Physiol* 2006;290(1):L120-6. doi: 10.1152/ajplung.00171.2005 [published Online First: 2005/08/30]
20. Seeherman H, Wozney JM. Delivery of bone morphogenetic proteins for orthopedic tissue regeneration. *Cytokine Growth Factor Rev* 2005;16(3):329-45. doi: 10.1016/j.cytogfr.2005.05.001 [published Online First: 2005/06/07]
21. Lo KW, Ulery BD, Ashe KM, et al. Studies of bone morphogenetic protein-based surgical repair. *Adv Drug Deliv Rev* 2012;64(12):1277-91. doi: 10.1016/j.addr.2012.03.014 [published Online First: 2012/04/20]
22. Kim NH, Cha YH, Kim HS, et al. A platform technique for growth factor delivery with novel mode of action. *Biomaterials* 2014;35(37):9888-96. doi: 10.1016/j.biomaterials.2014.08.005 [published Online First: 2014/09/15]
23. Kabouridis PS. Biological applications of protein transduction technology. *Trends Biotechnol* 2003;21(11):498-503. doi: 10.1016/j.tibtech.2003.09.008 [published Online First: 2003/10/24]
24. Kim S, Jeong C-H, Song SH, et al. Micellized Protein Transduction Domain-Bone Morphogenetic Protein-7 Efficiently Blocks Renal Fibrosis Via Inhibition of Transforming Growth Factor-Beta-Mediated Epithelial-Mesenchymal Transition. *Frontiers in Pharmacology* 2020;11 doi: 10.3389/fphar.2020.591275
25. Cho K, Kim NH, Seo SH, et al. A micellized bone morphogenetic protein-7 prodrug ameliorates liver fibrosis by suppressing transforming growth factor- β signaling. *Am J Cancer Res* 2022;12(2):763-78. [published Online First: 2022/03/10]
26. Leem AY, Shin MH, Douglas IS, et al. All-trans retinoic acid attenuates bleomycin-induced pulmonary fibrosis via downregulating EphA2-EphrinA1 signaling. *Biochem Biophys Res Commun* 2017;491(3):721-26. doi: 10.1016/j.bbrc.2017.07.122 [published Online First: 2017/07/27]
27. Ashcroft T, Simpson JM, Timbrell V. Simple method of estimating severity of pulmonary fibrosis on a numerical scale. *Journal of Clinical Pathology* 1988;41(4):467-70. doi: 10.1136/jcp.41.4.467

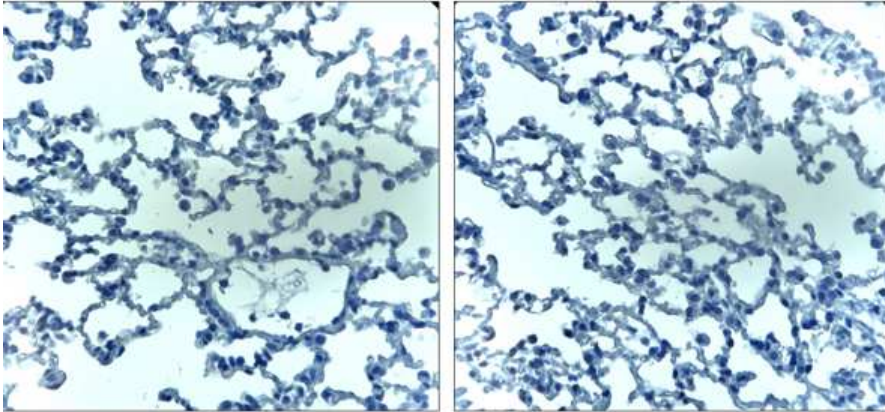
28. Reyfman PA, Walter JM, Joshi N, et al. Single-Cell Transcriptomic Analysis of Human Lung Provides Insights into the Pathobiology of Pulmonary Fibrosis. *Am J Respir Crit Care Med* 2019;199(12):1517-36. doi: 10.1164/rccm.201712-2410OC [published Online First: 2018/12/18]
29. Zhou BW, Liu HM, Xu F, et al. The role of macrophage polarization and cellular crosstalk in the pulmonary fibrotic microenvironment: a review. *Cell Commun Signal* 2024;22(1):172. doi: 10.1186/s12964-024-01557-2 [published Online First: 2024/03/10]
30. Mould KJ, Barthel L, Mohning MP, et al. Cell Origin Dictates Programming of Resident versus Recruited Macrophages during Acute Lung Injury. *Am J Respir Cell Mol Biol* 2017;57(3):294-306. doi: 10.1165/rcmb.2017-0061OC [published Online First: 2017/04/20]
31. Cui H, Jiang D, Banerjee S, et al. Monocyte-derived alveolar macrophage apolipoprotein E participates in pulmonary fibrosis resolution. *JCI Insight* 2020;5(5) doi: 10.1172/jci.insight.134539 [published Online First: 2020/02/07]
32. Shi X, Chen Y, Liu Q, et al. LDLR dysfunction induces LDL accumulation and promotes pulmonary fibrosis. *Clin Transl Med* 2022;12(1):e711. doi: 10.1002/ctm2.711 [published Online First: 2022/01/28]
33. Romero F, Shah D, Duong M, et al. A pneumocyte-macrophage paracrine lipid axis drives the lung toward fibrosis. *Am J Respir Cell Mol Biol* 2015;53(1):74-86. doi: 10.1165/rcmb.2014-0343OC [published Online First: 2014/11/20]
34. Zhu L, Fu X, Chen X, et al. M2 macrophages induce EMT through the TGF- β /Smad2 signaling pathway. *Cell Biology International* 2017;41(9):960-68. doi: <https://doi.org/10.1002/cbin.10788>
35. Remmerie A, Scott CL. Macrophages and lipid metabolism. *Cell Immunol* 2018;330:27-42. doi: 10.1016/j.cellimm.2018.01.020 [published Online First: 2018/02/13]
36. Yao X, Gordon EM, Figueroa DM, et al. Emerging Roles of Apolipoprotein E and Apolipoprotein A-I in the Pathogenesis and Treatment of Lung Disease. *Am J Respir Cell Mol Biol* 2016;55(2):159-69. doi: 10.1165/rcmb.2016-0060TR [published Online First: 2016/04/14]
37. Feingold KR, Shigenaga JK, Kazemi MR, et al. Mechanisms of triglyceride accumulation in activated macrophages. *Journal of Leukocyte Biology* 2012;92(4):829-39. doi:

10.1189/jlb.1111537

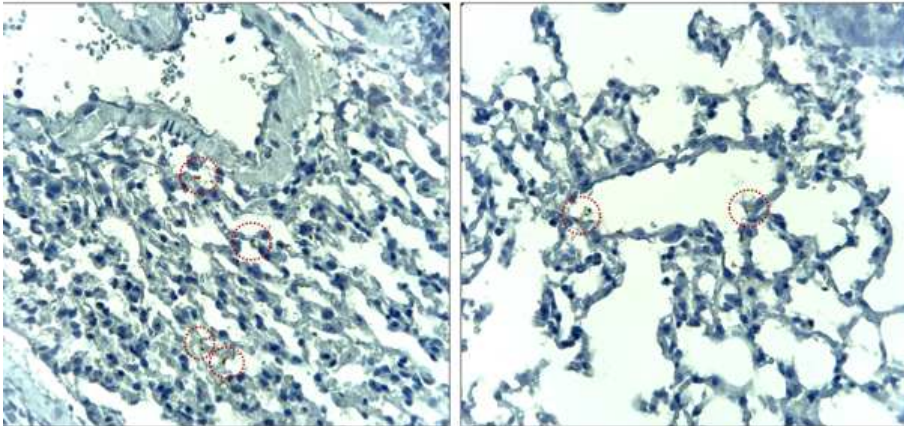
38. Odegaard JI, Chawla A. Alternative Macrophage Activation and Metabolism. *Annual Review of Pathology: Mechanisms of Disease* 2011;6(Volume 6, 2011):275-97. doi: <https://doi.org/10.1146/annurev-pathol-011110-130138>
39. Lv J, Gao H, Ma J, et al. Dynamic atlas of immune cells reveals multiple functional features of macrophages associated with progression of pulmonary fibrosis. *Front Immunol* 2023;14:1230266. doi: 10.3389/fimmu.2023.1230266 [published Online First: 2023/09/29]
40. Duerr GD, Dewald D, Schmitz EJ, et al. Metallothioneins 1 and 2 Modulate Inflammation and Support Remodeling in Ischemic Cardiomyopathy in Mice. *Mediators Inflamm* 2016;2016:7174127. doi: 10.1155/2016/7174127 [published Online First: 2016/07/13]
41. Dai H, Wang L, Li L, et al. Metallothionein 1: A New Spotlight on Inflammatory Diseases. *Frontiers in Immunology* 2021;12 doi: 10.3389/fimmu.2021.739918
42. Yang L, Gao JY, Ma J, et al. Cardiac-specific overexpression of metallothionein attenuates myocardial remodeling and contractile dysfunction in l-NAME-induced experimental hypertension: Role of autophagy regulation. *Toxicol Lett* 2015;237(2):121-32. doi: 10.1016/j.toxlet.2015.06.005 [published Online First: 2015/06/13]
43. Okamoto T, Mathai SK, Hennessy CE, et al. The relationship between complement C3 expression and the MUC5B genotype in pulmonary fibrosis. *Am J Physiol Lung Cell Mol Physiol* 2018;315(1):L1-110. doi: 10.1152/ajplung.00395.2017 [published Online First: 2018/03/23]
44. Addis-Lieser E, Köhl J, Chiaramonte MG. Opposing regulatory roles of complement factor 5 in the development of bleomycin-induced pulmonary fibrosis. *J Immunol* 2005;175(3):1894-902. doi: 10.4049/jimmunol.175.3.1894 [published Online First: 2005/07/22]

APPENDICES

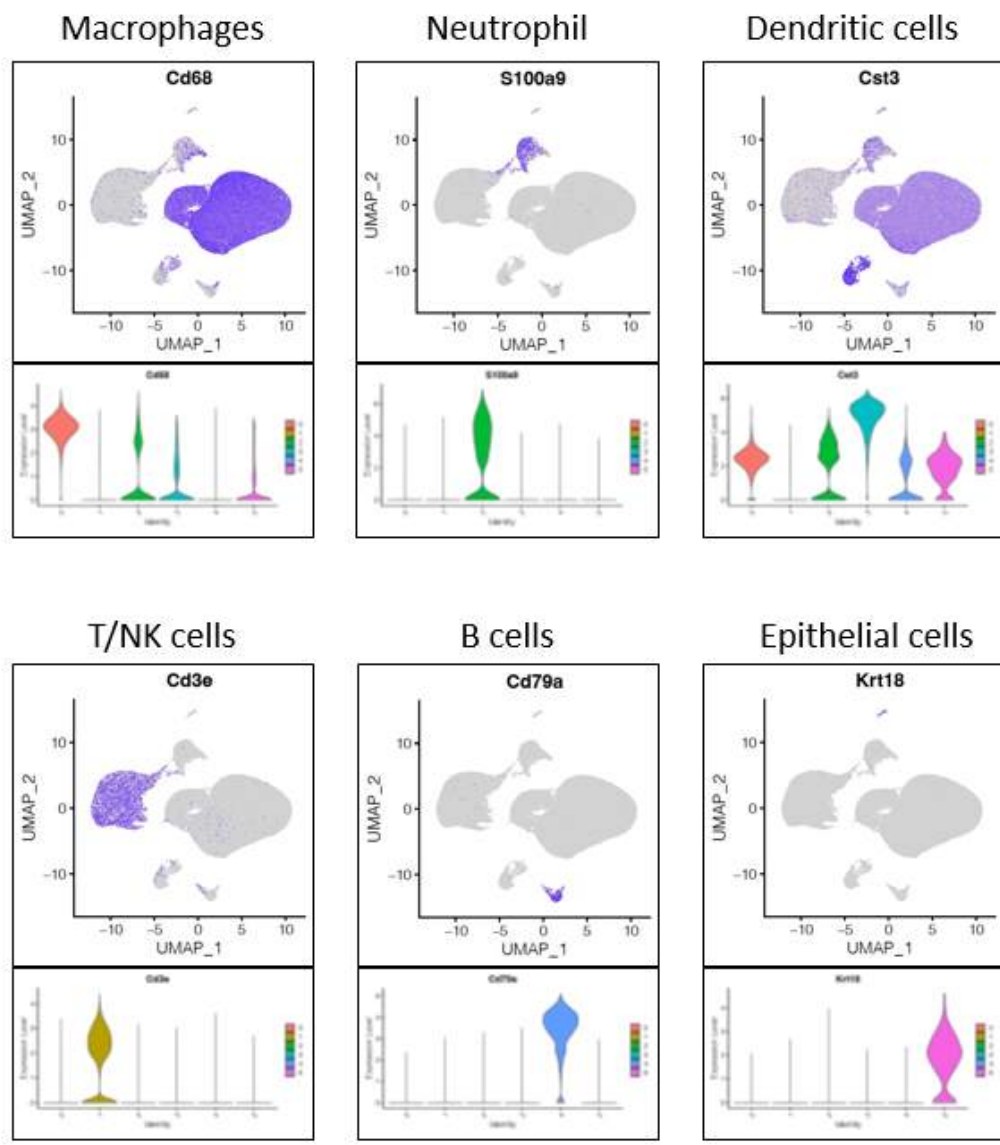
A)



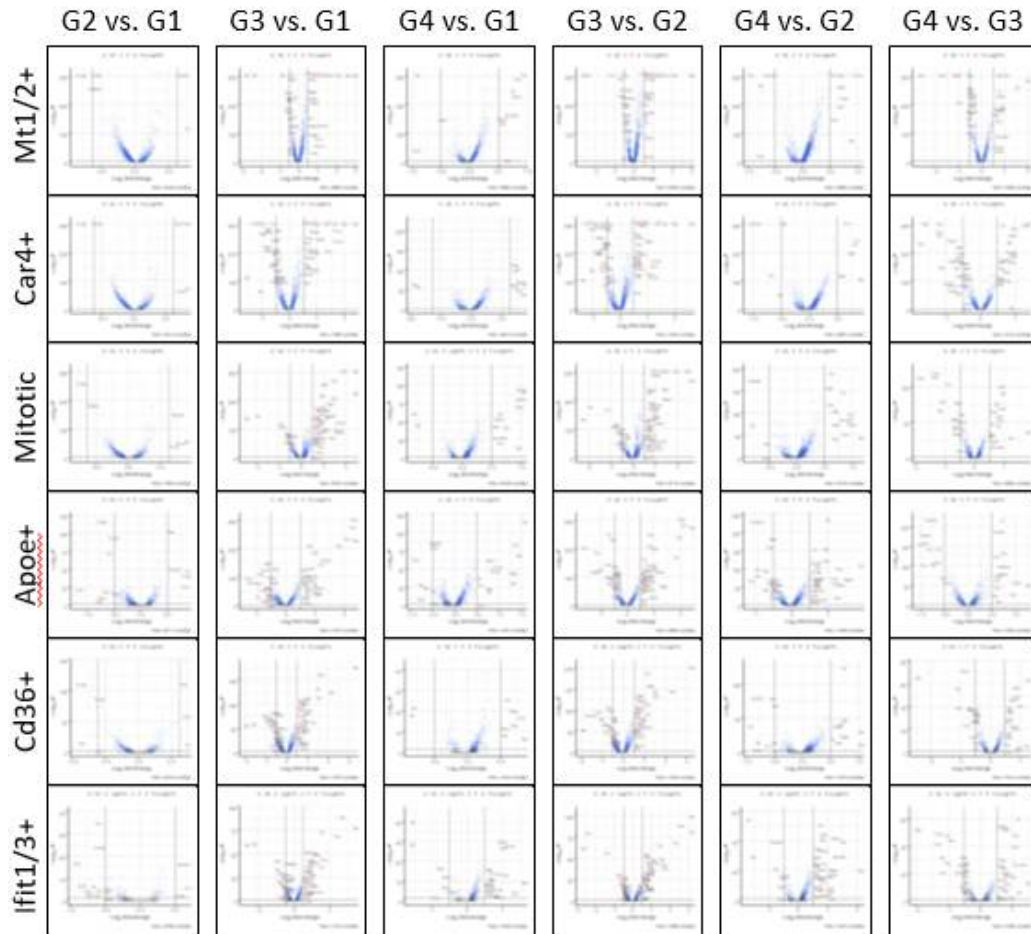
B)



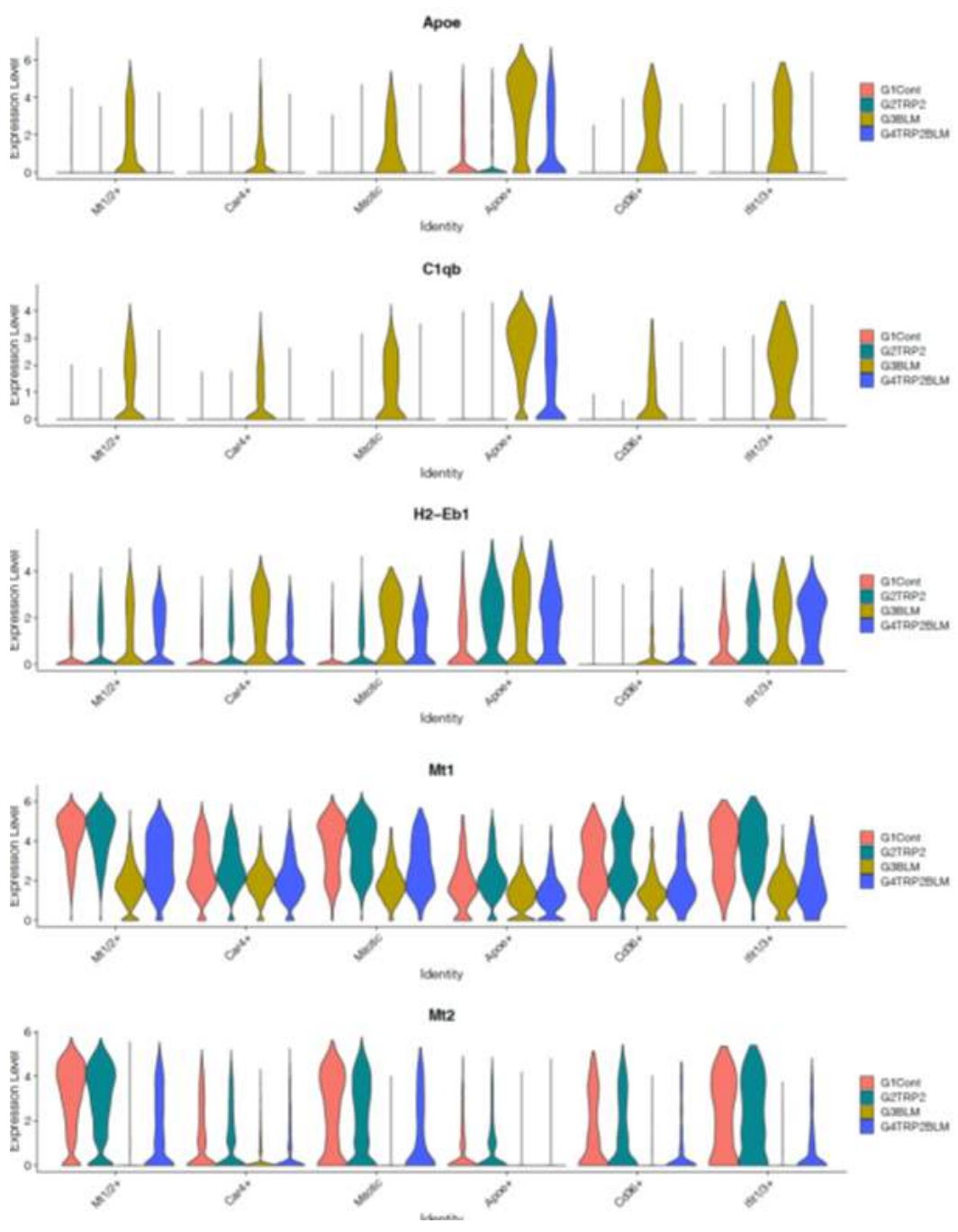
Supplementary Figure 1. Immunostaining of prodrug BMP-7 in the lungs of a group of mice. A) A group of mice inhaled with a vehicle. B) A group of mice inhaled the prodrug BMP-7, prodrug BMP-7 immunostaining shown at bronchioles or alveolar sacs (shown in red dots).



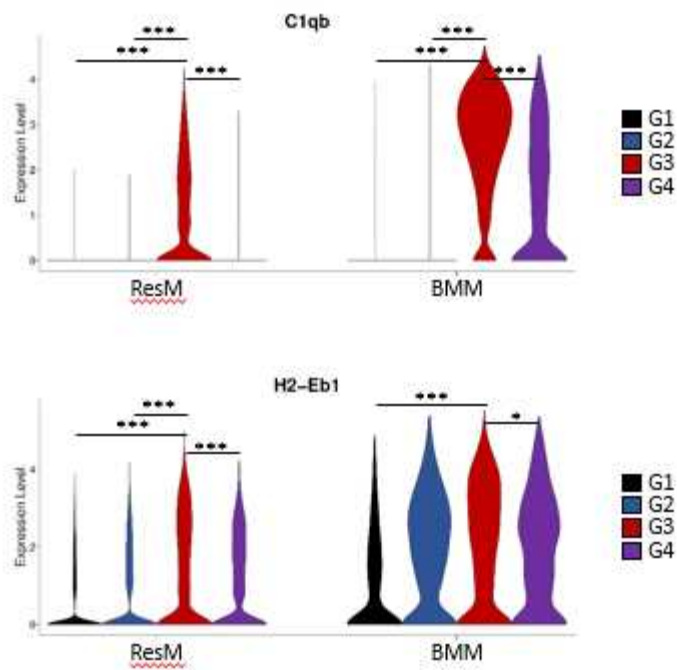
Supplementary Figure 2. Feature and violin plots of marker gene expression in cell clusters.



Supplementary Figure 3. Volcano plots illustrating differentially expressed genes in six macrophage subclusters: Mt1/2+, Car4+, mitotic, ApoE+, Cd36+, Ifit1/3+, between two selected groups from G1, G2, G3, and G4.

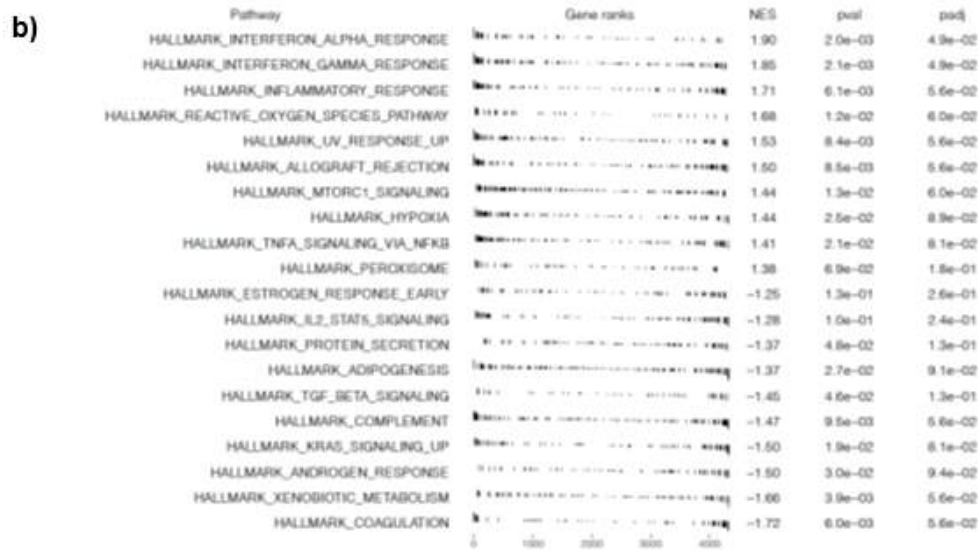
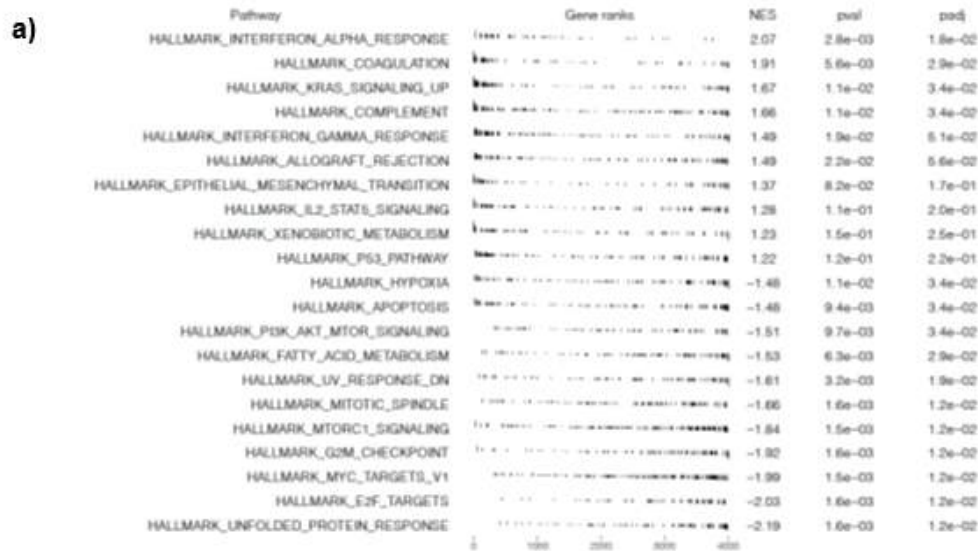


Supplementary Figure 4. Violin plots of gene expression across macrophage subclusters and groups.

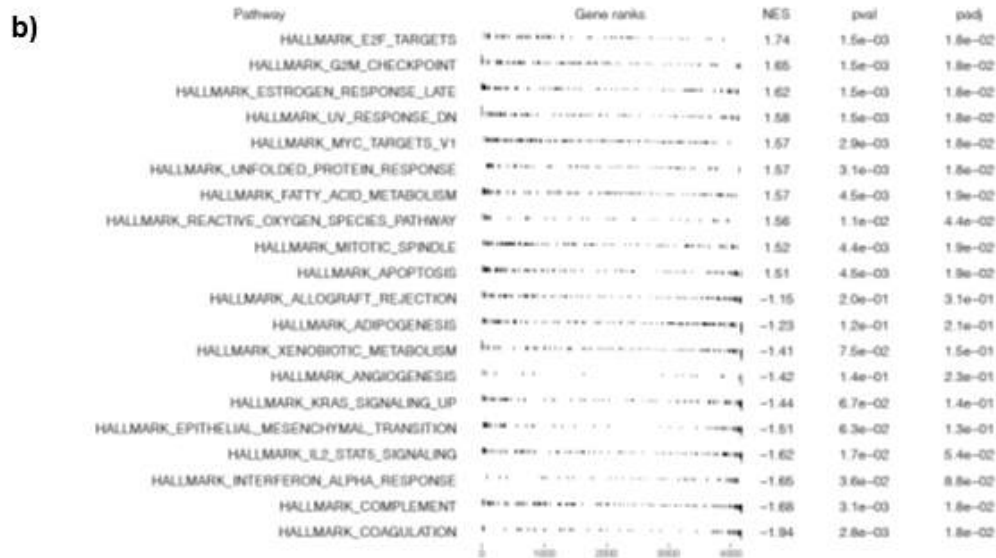
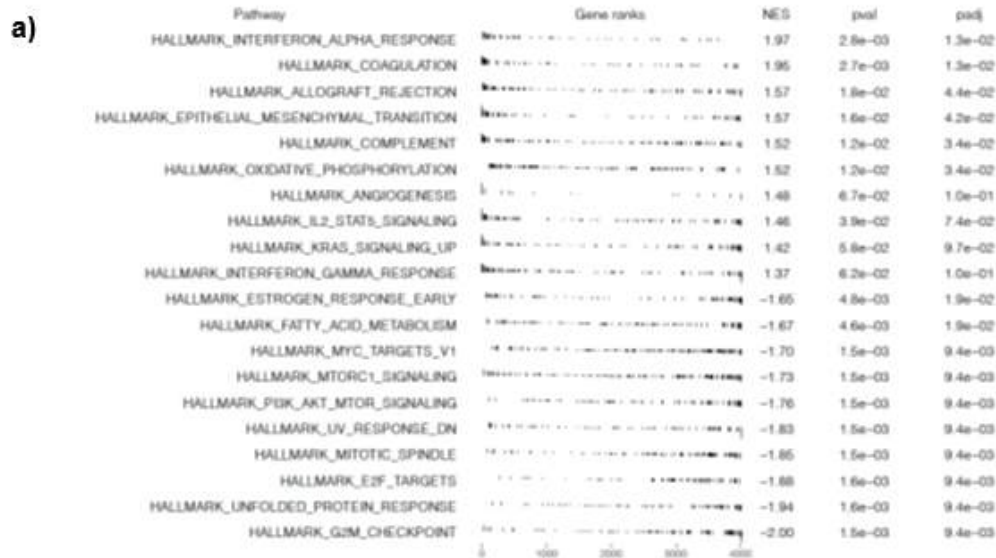


Supplementary Figure 5. Violin plots of C1qb and H2-Eb1 gene expression in ResM and BMM across each group.

* $P < 0.05$; ** $P < 0.01$; and *** $P < 0.001$.



Supplementary Figure 6. GSEA results for BMM according to the MSigDB Hallmark gene sets. GSEA of 10 upregulated/downregulated genes in a) G3 compared with G1 and b) G4 compared with G3.



Supplementary Figure 7. GSEA results for ResM according to the MSigDB Hallmark gene sets. GSEA of 10 upregulated/downregulated genes in a) G3 compared with G1 and b) G4 compared with G3.

Supplement documents

Isolation of bronchoalveolar lavage cells and cell counts

At 21 days after BLM/PBS instillation, all mice were humanely euthanized by lethal overdose of ketamine and xylazine. BALF was collected through a tracheal cannula using two 1 ml aliquots of sterile saline. Subsequently, samples were centrifuged for 10 min at 4°C and 1,500–5,000 rpm. The resulting cell pellet was resuspended in 100 µL of PBS and analyzed by quantitative and qualitative cell counting. Cells were counted using a hemocytometer According to the manufacturer's protocol (Marienfield, Germany). Slide chambers were prepared by inserting slides into frames with the poly-L-lysine coating up and clamping with clips on either side. A 90 µl aliquot of each sample was inserted into a cytospin with slides facing outward, filled with 90 µL of the sample, and centrifuged at 600 rpm for 6 min. The slides were then retrieved, dried, and stained by immersing in Diff-Quick (Sysmex Corporation). The slides were immersed in three Diff Quick fluids (Fixative, Solution I, and Solution II) for 5 s and rinsed with purified water. The protein content of the BAL supernatant was measured using the Coomassie Brilliant Blue G-250 technique (Quick Start™ Bradford Protein Assay). In addition, 25 µl of each sample and 200 µl of the working reagent were pipetted into a microplate well and mixed thoroughly on a plate shaker for 30 s. After incubation for 30 min at 37°C, the plate was cooled, and the absorbance was read at 562 nm using a spectrophotometer.

Lung tissue harvest and histological examination

The right lung was isolated and stored at –80°C before protein extraction after flushing the pulmonary vasculature with saline at low pressure. The left lung was inflated *via* tracheotomy with low-melting-point agarose (4%) in PBS at 25 cm H₂O pressure until the pleural margins became sharp. Subsequently, tissues were excised, fixed overnight in 10% formaldehyde in PBS, embedded in paraffin, and sectioned at 5 µm. The sections were stained with H&E and Masson's trichrome and scored under a light microscope by two qualified investigators blinded to the samples. Fibrotic changes in lung sections were graded semiquantitatively according to the scale defined by the modified Ashcroft score.²⁷

All lung parenchyma sections were assessed using a score of 0–8. In every field, fibrosis was recorded as predominant when it occupied more than half of the area. The final score was expressed as the mean of the individual scores observed in all fields.

Western blotting

The frozen lungs were mechanically homogenized in 600 μ L with homogenization buffer (PRO-PREPTM Extraction Solution), and cell lysis was induced by incubation for 20–30 min on ice or at -20°C . The samples were then centrifuged at $13,000 \times g$ for 30 min at 4°C . Equal amounts of protein were separated using SDS-PAGE and transferred to nitrocellulose membranes before immunoblotting with primary antibodies. Subsequently, membranes were incubated with anti-rabbit or anti-mouse IgG conjugated to horseradish peroxidase and visualized using SuperSignal West Pico Chemiluminescence Detection Kit (Pierce). The band images were quantified using AlphaEase FC version 4.1.0 (Innotech). The antibodies used in this study included α -SMA (Abcam #ab7817, 1:2,000), collagen I (Abcam #ab34710, 1:2,000), fibronectin (Abcam #ab2413, 1:2,000), β -actin (Santa Cruz #sc-47778, 1:1,000), p-smad2/3 (cell signaling #8828, 1:500), and Smad2/3 (cell signaling #3102, 1:500).

Single-cell RNA-seq analysis of BAL fluid cells

BAL fluid single cells were collected and pooled for each group. In total, 40,000 cells per group were loaded onto microwell cartridges of the BD Rhapsody Express system (BD). Single-cell whole transcriptome analysis libraries were prepared using BD Rhapsody WTA Reagent kit (BD: 633802) according to the manufacturer's instructions. The final index PCR libraries were sequenced on Illumina HiSeq using High Output Kit v2.5 (150 cycles, Illumina) for 2×75 bp paired-end reads with an 8 bp single index.

The FASTQ-format sequencing raw data were processed using the BD Rhapsody WTA Analysis pipeline (version 1.0, Revision 6) on the SevenBridges Genomics online platform (SevenBridges), and the expression matrix was used for further data analysis.

Unless otherwise specified, data normalization, dimensionality reduction, and visualization were performed using the Seurat package (version 4.3.0).

Cells were filtered based on the following criteria to ensure data quality: having 500–6,000 genes per cell (nFeature_RNA) and a percentage of mitochondrial genes (percent.mito) of <25. In addition, genes were filtered to include only those present in a minimum of three cells. After filtering, the matrices were normalized using the NormalizeData function with the LogNormalize method and a scale factor of 10,000. Variable genes were identified using the FindVariableFeatures function, selecting the top 2,000 genes using the variance stabilizing transformation method, excluding genes related to the cell cycle (GO: 0007049). Data integration was achieved using the FindIntegrationAnchors and IntegrateData functions with default options. The integrated data were further processed using the ScaleData and RunPCA functions. Statistically significant principal components were identified using the JackStraw method, which were subsequently used for UMAP nonlinear dimensional reduction.

The FindClusters function in the Seurat package was applied for the unsupervised hierarchical clustering analysis. Various resolutions of 0.1–0.9 were tested; the final resolution was selected based on the most stable and relevant outcome, using the clustree R package and considering prior knowledge. The cellular identity of each cluster was determined by finding cluster-specific marker genes using the FindAllMarkers function. Marker genes were considered with a minimum fraction of cells expressing the gene over 25% (min.pct = 0.25). Comparisons were made against known cell type-specific genes from PanglaoDB (<https://panglaoDB.se>).

DEGs were identified using the FindMarkers function of the Seurat package with logfc.threshold = 0. GSEA was performed using the Molecular Signatures Database (MSigDB) with the fgsea R package [Korotkevich, G., Sukhov, V. & Sergushichev, A. Fast GSEA. Preprint at BioRxiv <https://doi.org/10.1101/060012> (2019)]. DEGs between different groups were identified using the FindMarkers function in Seurat with min.pct = 0.25 and logfc.threshold = 0, preranked according to the average log₂ fold change values, and used for enriched gene set identification using the gfsea function with minSize = 15, maxSize = 500, and nperm = 1,000 options.

Immunofluorescence and immunohistochemistry staining

Unstained mouse lung tissue slides embedded in 5 μm formalin-fixed paraffin blocks were deparaffinized and washed three times with PBS. Subsequently, the slides were incubated in 1% citrate buffer (pH: 8.0) at 95°C–98°C for 45 min to facilitate antigen retrieval. After two additional washes with PBS, permeabilization was performed using 1% SDS for 10 min.

Following permeabilization, the primary antibodies, ApoE recombinant rabbit monoclonal (Thermo Fisher Scientific, Catalog No. 701241), and the macrophage marker, CD68 (Santa Cruz Biotherapy, Inc., Catalog No. sc-20060), were diluted in DAKO antibody dilution buffer (1:1,000) and incubated overnight at 4°C. Goat anti-rabbit IgG secondary antibody, Alexa Fluor™ 488, or goat anti-mouse IgG secondary antibody, Alexa Fluor™ 568 (Invitrogen), was diluted 1:1,000 and incubated for 1 h at room temperature. Subsequently, the secondary antibodies were washed with PBS, and the nuclei were stained with 1 $\mu\text{g}/\text{ml}$ DAPI for 20 min.

Fluorescence images were captured using a Zeiss LSM700 confocal microscope (Carl Zeiss, Berlin, Germany). Morphological analysis of the acquired confocal images was performed using Metamorph microscopy analysis software (version 7.1, Molecular Devices, Sunnyvale, CA, USA). Twenty-four-bit confocal images were used for image quantification under each condition

Prodrug BMP-7의 골수 유래 Apo E+ 폐포 대식세포 조절을 통한 항섬유화 효과

Bone morphogenetic Protein-7 (BMP-7)은 폐섬유화에 결정적으로 관여하는 Transforming Growth Factor- β (TGF- β)를 길항 한다. 본 연구에서는 나노입자로 설계된 prodrug BMP-7이 Bleomycin (BLM) 폐섬유증 마우스 모델에서 항섬유화 효과를 나타내는지 분석하고, 폐포 대식세포에 대한 prodrug BMP-7의 역할을 규명하기 위해 bronchoalveolar lavage fluid (BALF) 단일 세포 RNA 시퀀싱을 수행했다.

38마리의 마우스 (C57BL/6)를 대조군, BLM 그룹, prodrug BMP-7 그룹으로 나누었으며, prodrug BMP-7과 vehicle은 각각 21일 동안 72시간 간격으로 흡입되었다. BLM 그룹에 비해 prodrug BMP-7 흡입 그룹에서 유의미한 섬유화 감소가 관찰되었으며, 마손삼색 염색 및 변형된 Ashcroft 폐 섬유증 채점 시스템을 사용하여 이를 증명하였다. Western blot에서 prodrug BMP-7 그룹의 collagen 1, α -SMA, fibronectin의 mRNA 감소, TGF- β /SMAD 하향조절이 관찰되었고, 마우스 폐 조직과 BALF에서의 CXCL10, CXCL2와 등의 케모카인 감소를 ELISA를 통해 확인했다. 다음으로, BALF 단일 세포 RNA 시퀀싱을 통해 Apo E+ 대식세포의 비율이 BLM 군에서 유의하게 증가하고 prodrug BMP-7에서는 유의하게 감소함을 관찰했으며, 특발성폐섬유증 환자의 폐 조직에서 ApoE 발현 증가와 BLM 폐섬유화증 마우스 모델에서 prodrug BMP-7 흡입 시 Apo E 발현의 감소를 확인했다.

이는 prodrug BMP-7이 Apo E+ 폐포 대식세포의 조절을 통해 폐섬유화에 대한 효과적인 치료제가 될 수 있음을 시사한다.

핵심되는 말 : prodrug BMP-7, Apo E+ 폐포 대식세포, 폐섬유화